pharmaceutics

MDPI

Article

CD44 Targeting of Cisplatin-Loaded Hyaluronic Acid-Modified Mesoporous Silica Nanoparticles for Lung Adenocarcinoma: Synthesis, Characterization, In Vitro and In Vivo Evaluation

Cem Güler [1], S. Sacide Gelen [2], Ebru Şancı [3], Aylin Buhur [4], H. Ece Tıkır [5], Ayşe Nalbantsoy [5], Adem Güner [6], E. İlker Medine [7], Altuğ Yavaşoğlu [8], Dilek Odacı [2] and N. Ülkü Karabay Yavaşoğlu [1,*]

1 Department of Biology, Faculty of Science, Ege University, Izmir 35100, Turkey; gulercem35@gmail.com
2 Department of Biochemistry, Faculty of Science, Ege University, Izmir 35100, Turkey; sacide.gelen@gmail.com (S.S.G.); dilek.odaci.demirkol@ege.edu.tr (D.O.)
3 Center for Drug R&D and Pharmacokinetic Applications, Ege University, Izmir 35100, Turkey; ebruusanci@gmail.com
4 Department of Basic Sciences, Faculty of Dentistry, Istanbul Galata University, Istanbul 34303, Turkey; ayln.bhr@gmail.com
5 Department of Bioengineering, Faculty of Engineering, Ege University, Izmir 35100, Turkey; ecetikir@gmail.com (H.E.T.); ayse.nalbantsoy@ege.edu.tr (A.N.)
6 Department of Occupational Health and Safety, Faculty of Health Sciences, Sinop University, Sinop 57000, Turkey; ademeguner@gmail.com
7 Department of Nuclear Applications, Institute of Nuclear Science, Ege University, Izmir 35100, Turkey; emin.ilker.medine@ege.edu.tr
8 Department of Histology and Embryology, Faculty of Medicine, Ege University, Izmir 35100, Turkey; altug.yavasoglu@ege.edu.tr
* Correspondence: ulku.karabay@ege.edu.tr

Abstract

Background/Objectives: Cisplatin (CDDP) is widely used in the treatment of non-small cell lung cancer (NSCLC); however, its clinical efficacy is limited by severe systemic toxicity. Hyaluronic acid (HA) modification enables the targeting of CD44-overexpressing cancer cells, enhances biocompatibility, provides controlled drug release, and prolongs systemic circulation. This study aimed to develop high-molecular-weight hyaluronic acid-modified, cisplatin-loaded mesoporous silica nanoparticles (HA-MSN-CDDP) to selectively target CD44-overexpressing lung adenocarcinoma cells. **Methods:** HA-MSN-CDDP nanoparticles were synthesized via the sol–gel method and characterized by FTIR, DLS, SEM, and TEM methods. Antitumor efficacy was evaluated using both in vitro and in vivo xenograft lung cancer models in mice. **Results:** HA modification enabled controlled and sustained release of cisplatin from the HA-MSN-CDDP drug delivery system. Through HA-mediated receptor-dependent endocytosis, the nanoparticles exhibited enhanced cellular uptake and selective cytotoxicity toward CD44-positive cells. HA-MSN-CDDP significantly reduced the cytotoxic, genotoxic, and oxidative stress effects of free cisplatin on healthy cells while markedly enhancing apoptosis in A549-Luc-C8 cells. The system showed excellent hemocompatibility, supporting its potential for intravenous use. In vivo, HA-MSN-CDDP effectively suppressed tumor growth, mitigated lipid peroxidation, and preserved antioxidant enzyme activities (SOD and CAT) in major organs. Histological analyses confirmed reduced cisplatin-induced nephrotoxicity. **Conclusions:** HA-MSN-CDDP demonstrates strong potential as a targeted chemotherapeutic platform for NSCLC, combining high antitumor efficacy with reduced systemic toxicity.

Keywords: cisplatin; mesoporous silica nanoparticles; hyaluronic acid; CD44; drug delivery system; active targeting; lung cancer

Academic Editor: Francisco Arriagada

Received: 31 October 2025
Revised: 30 November 2025
Accepted: 2 December 2025
Published: 28 January 2026

1. Introduction

Lung cancer is one of the most aggressive malignancies and remains the leading cause of cancer-related deaths worldwide. It is classified into two main histological subtypes, small-cell lung cancer (SCLC) and non-small-cell lung cancer (NSCLC), the latter accounting for approximately 85% of all lung cancer cases. NSCLC includes three major subtypes: adenocarcinoma, squamous cell carcinoma, and large cell carcinoma [1]. Current treatment options for lung cancer include surgery, radiotherapy, chemotherapy, immunotherapy, and molecularly targeted therapies. Although surgical resection can be highly effective, it is often not feasible due to late-stage diagnosis, tumor invasion, or metastasis. For this reason, chemotherapeutic agents with strong cytotoxic activity are commonly used to manage NSCLC [2]. However, conventional chemotherapeutics often exhibit poor water solubility due to their hydrophobic nature, necessitating high doses for therapeutic efficacy. Moreover, their lack of tumor specificity results in poor bioavailability and severe toxic effects on healthy tissues [3]. To overcome these limitations, nanoparticle (NP)-based smart drug delivery systems have been developed to enhance the therapeutic performance and safety of chemotherapeutic agents. NPs are highly suitable for biomedical applications, particularly in oncology, owing to their small size, large surface area, and high surface energy. They can encapsulate and protect drugs from premature degradation, enhance solubility and bioavailability, and enable controlled and targeted delivery. This approach allows for a reduction in the required drug dose and minimizes adverse side effects by selectively targeting cancer cells. Both organic and inorganic nanoparticles, including mesoporous silica nanoparticles (MSNs), have been widely investigated for drug delivery applications in cancer therapy, including lung cancer [4–6].

MSNs are biocompatible and biodegradable inorganic NPs characterized by a high surface area, large pore volume, tunable pore size, thermal stability, and high drug-loading capacity. These properties make them excellent candidates for use in bioimaging, biosensing, therapy, diagnostics, tissue engineering, and particularly in drug delivery [6,7]. They can be synthesized by various methods such as hydrothermal synthesis, microemulsion templating, and the sol–gel method. Factors such as surfactant type and synthesis conditions significantly influence the physicochemical characteristics of MSNs, including particle size and morphology as well as pore size and structure [7]. Typically, MSNs are synthesized using tetraethyl orthosilicate (TEOS) via the sol–gel method, with particle sizes ranging between 50 and 300 nm. These structural parameters are critical for achieving optimal drug loading and release profiles in drug delivery applications. The ease of surface modification further enhances their potential for targeted drug delivery. Functionalization can be achieved through the silanol groups present on the MSN surface, forming stable Si–O bonds that provide stability to MSN against degradation and mechanical stress. Surface modification allows for the attachment of targeting ligands, enabling site-specific delivery to tumor tissues [8,9]. Common targeting moieties include transferrin, folic acid, and, notably, hyaluronic acid [7,8].

Hyaluronic acid (HA) is a natural, linear polysaccharide belonging to the glycosaminoglycan family. It consists of repeating disaccharide units of D-glucuronic acid and N-acetyl-D-glucosamine linked via β-(1 → 3) and β-(1 → 4) glycosidic bonds. HA is abundant in the extracellular matrix of connective tissues, including the skin, synovial fluid, vitreous humor, umbilical cord, and joint structures such as tendons, pleura, and pericardium [10]. It can be derived from both animal and microbial sources, although animal-derived HA may trigger allergic reactions. Based on molecular weight, HA is classified as low-molecular-weight (LMWHA, 10–500 kDa) or high-molecular-weight (HMWHA, >500 kDa) [11]. Owing to its biocompatibility, biodegradability, and non-immunogenic nature, HA is widely used in orthopedics, ophthalmology, aesthetic dermatology, and oncology [10]. The CD44 receptor,

a cell surface glycoprotein, is associated with tumor progression, metastasis, and drug resistance. HA specifically recognizes and binds to CD44, making it an effective targeting ligand for CD44-overexpressing cancer cells, including lung cancer. In addition, HA enhances nanoparticle biocompatibility and prolongs systemic circulation by conferring a negative surface charge [12,13]. While LMWHA has been extensively used for nanoparticle functionalization [14–20], recent studies highlight the superior performance of HMWHA, which offers enhanced anticancer efficacy while reducing chemotherapeutic side effects [21–25].

Cisplatin (CDDP) is a widely used, water-soluble, metal-based chemotherapeutic agent administered intravenously. Its cytotoxic mechanism involves binding to purine bases in DNA, forming DNA adducts that disrupt replication and transcription, arrest the cell cycle at the G1, S, or G2/M phases, and ultimately induce apoptosis. However, due to its lack of tumor selectivity, cisplatin also damages healthy tissues, leading to severe side effects such as hepatotoxicity, neurotoxicity, cardiotoxicity, and nephrotoxicity [26,27]. Despite these limitations, cisplatin remains a first-line chemotherapeutic for various cancers, including lung cancer. Notably, A549 human lung adenocarcinoma cells overexpress CD44 receptors [16], making them suitable targets for HA-mediated delivery systems. In this study, we developed a novel high-molecular-weight hyaluronic acid-functionalized, cisplatin-loaded mesoporous silica nanoparticle (HA-MSN-CDDP) system designed to target CD44-overexpressing lung cancer cells. The aim was to enhance the antitumor efficacy of cisplatin while minimizing its systemic toxicity. The therapeutic performance of HA-MSN-CDDP was evaluated through comprehensive in vitro and in vivo xenograft lung cancer models.

2. Materials and Methods

2.1. Reagents and Chemicals

Hexadecyltrimethylammonium bromide (CTAB) (Sigma H5882, St. Louis, MO, USA), tetraethyl orthosilicate (TEOS, MW: 208.33 g/mol) (Sigma 86578, Schnelldorf, Germany), 3-Aminopropyltriethoxysilane (APTES) (Sigma 440140, St. Louis, MO, USA), triethanolamine (TEA) (Sigma 90279, Schnelldorf, Germany), Cisplatin (Hospira, Warwickshire, UK), hyaluronic acid sodium salt from *Streptococcus equi* (HA, ~1.5–1.8 MDa), Sigma 53747, St. Louis, MO, USA), N-(3-dimethylaminopropyl)-N-ethylcarbodiimide hydrochloride (EDC, Sigma E7750, St. Louis, MO, USA), N-Hydroxysuccinimide (NHS, Sigma 56480, Schnelldorf, Germany), methanol (Merck 106009, Darmstadt, Germany), phosphate-buffered saline (PBS) tablets (Bioshop PBS404.100, Burlington, ON, Canada), Histopaque®-1077 (Sigma 10771, St. Louis, MO, USA), dialysis tubing cellulose (Sigma D9277, Schnelldorf, Germany), DMEM F12 (Gibco 11-320-033, St. Louis, MO, USA), RPMI-1640 (Gibco 11,875,093, USA), Fetal Bovine Serum (FBS) (Sigma F7524, St. Louis, MO, USA), penicillin/streptomycin (Biochrom A2213, Berlin, Germany), Thiazolyl Blue Tetrazolium Bromide (MTT) (Applichem A2231, Darmstadt, Germany), Rhodamine B (Sigma Aldrich R6626, Darmstadt, Germany), Hoechst 33342 (Sigma B2261, St. Louis, MO, USA), Annexin V-FITC/PI Apoptosis Kit (Elabscience E-CK-A211, St. Louis, MO, USA), LDH assay kit (Cayman Chemical Company 601170, Ann Arbor, MI, USA), Triton X-100 (Sigma T8787, St. Louis, MO, USA), Total Oxidant Status Assay Kit (TOS kit) (Rel Assay Diagnostics, Gaziantep, Turkey), hydrogen peroxide (H_2O_2) (Merck, 108600, Darmstadt, Germany), Chromosome medium B (Biochrom F5023, Berlin, Germany), potassium chloride (KCl) (Sigma P-4504, Darmstadt, Germany), acetic acid (Merck 100063, Darmstadt, Germany), phytohemagglutinin (Biological Industries 12-006-1H, St. Louis, MO, USA), Cytochalasin B (Sigma C6762, St. Louis, MO, USA), dimethyl sulfoxide (DMSO) (Sigma D8418, St. Louis, MO, USA), phenylmethanesulfonylfloride (PMSF) (Sigma P7626, Beijing, China), DL-Dithiothreitol (DTT) (Sigma D0632, Steinheim, Germany), 2-Thiobarbituric acid (TBA) (Sigma T5500, Darmstadt, Germany), IVISense Vascular 680 Fluorescent Probe (AngioSense)

(Revvity Health Sciences Inc. NEV10054EX, Waltham, MA, USA), Anti-Ki-67 Antibody (Sigma AB9260, Strasbourg, France).

2.2. Synthesis of Nanoparticles

2.2.1. Synthesis of Mesoporous Silica Nanoparticles (MSNs)

MSNs were synthesized according to the method described by Ichedef et al. (2021) [28]. Briefly, 2 g of CTAB and 140 µL of TEA were dissolved in ultrapure water (UPW) and stirred for 1 h at 95 °C. After the reaction mixture reached equilibrium, 3 mL of TEOS was added dropwise, and the solution was stirred for an additional 1 h to allow silica condensation. The resulting suspension was washed with ethanol and centrifuged twice at 10,000 rpm for 15 min to remove excess surfactant and byproducts. Subsequently, the obtained precipitate was dispersed in 20 mL of methanol containing 1 mL of HCl and stirred overnight at 60 °C to remove the CTAB template. The product was washed twice with methanol, and this extraction step was repeated to ensure complete removal of residual surfactant. Finally, the purified MSNs were dried in an oven at 50 °C to obtain the final MSN powder.

2.2.2. Synthesis of HA-Modified MSN (HA-MSN)

MSNs were dispersed in 30 mL of ethanol containing 500 µL of APTES for functionalized with amine groups and stirred overnight at 80 °C. Following the reaction, the mixture was centrifuged at 10,000 rpm for 15 min and washed twice with ethanol and once with acetone to remove unreacted reagents. The obtained amino-functionalized nanoparticles (MSN-NH_2) were dried in an incubator at 37 °C. HA conjugation was performed according to the method of Yu et al. (2013) [14]. MSN-NH_2 (100 mg) was dispersed in 10 mL of UPW. Separately, 37 mg of NHS, 20 mg of EDC, and 6 mg of HA (~1.5–1.8 MDa) were dissolved in 8 mL of UPW and stirred at 550 rpm for 15 min at room temperature to activate the carboxyl groups of HA. The activated HA solution was then added to the MSN-NH_2 suspension and stirred for 4 h at 550 rpm at room temperature. The resulting HA-modified nanoparticles (HA-MSNs) were collected by centrifugation at 10.000 rpm for 15 min (three washing cycles with UPW), followed by drying at 37 °C.

2.2.3. Cisplatin (CDDP) Loading

CDDP was loaded into MSNs and HA-MSNs using the method by Huang et al. (2018) [29]. In total, 40 mg nanoparticles were added to 20 mL CDDP solution (1 mg/mL concentration) and stirred in dark at 200 rpm, 37 °C for 24 h. After the reaction they were washed twice with distilled water at 10.000 rpm for 30 min. Then, the NPs were dried in the incubator at 37 °C. To calculate CDDP loading efficiency, the supernatant was collected, and CDDP content was measured in UV–vis spectrophotometer at 215 nm. Finally, drug adsorption capacity was calculated with the equation:

$$Q = \left(C_i - C_f\right) \times \frac{V}{m} \quad (1)$$

where Q, adsorption capacity; Ci, initiation concentration of drug; Cf, free drug concentration; V, volume of reaction medium; and m, nanoparticle dry mass.

2.3. Characterizations

The synthesized nanoparticles (MSN, HA-MSN, MSN-CDDP, and HA-MSN-CDDP) were characterized using Fourier transform infrared spectroscopy (FTIR), dynamic light scattering (DLS), scanning electron microscopy (SEM), and transmission electron microscopy (TEM). FTIR spectra were recorded using an FTIR spectrophotometer (IRTracer-100, SHIMADZU, İstanbul, Turkey) in the range of 400–4000 cm^{-1} at 25 °C to identify the functional groups and confirm surface modifications. The hydrodynamic diameter and zeta

potential of the nanoparticles were determined by DLS (Malvern Nano-ZS, Malvern, UK) in distilled water at 25 °C. The particle size distribution, surface morphology, and structural features of the nanoparticles were examined using SEM (Thermo Scientific Apreo S, Waltham, MA, USA) and TEM (Hitachi HT7800, Tokyo, Japan).

2.4. In Vitro Drug Release

The release of cisplatin from MSN-CDDP and HA-MSN-CDDP was evaluated in vitro conditions under pH 7.4 and 5.5 [29]. Dialysis bags (MWCO 14.000 Da) contained 0.5 mL samples of MSN-CDDP and HA-MSN-CDDP suspension and free CDDP solution. Then, the dialysis bags were placed in PBS solution (20 mL, pH 7.4 and 5.5) and stirred at 100 rpm in dark at 37 °C. To calculate releasing amount of the drug, 1 mL release medium was collected from releasing medium at predetermined time intervals and measured at 215 nm by UV–vis spectrophotometer (Agilent BioTek Epoch 2, Santa Clara, CA, USA).

2.5. In Vitro Assays

2.5.1. Cell Culture

A549-Luc-C8 (Luciferase-expressing human non-small cell lung carcinoma, CVCL-5J13) and CCD-34Lu (Human lung fibroblast cells, ATCC-CRL-1491™) were cultured in Dulbecco's Modified Eagle's Medium (DMEM) Ham's F12. PBMCs (human primary peripheral blood mononuclear cells, ATCC-PCS-800-011™) were cultured in RPMI-1640 medium. These media contain 10% fetal bovine serum (FBS), 2 mM L-glutamine, 100 U/mL of penicillin, and 100 µg/mL of streptomycin (5% CO_2 and 37 °C).

2.5.2. Cellular Uptake

Cellular uptake of the HA-MSN was confirmed by fluorescent microscope via fluorescent dye labeling of the NPs [30]. MSN was prepared at 1 mg/mL. Then, Rhodamine B (ratio of 1:100 according to NPs) was added to the reaction for labeling the NPs and stirring for 2 h in dark. To remove unbound dye, the NPs were washed with distilled water three times at 10,000 rpm for 20 min. Rhodamine B-labeled MSN was dried overnight in a 37 °C oven to obtain powder. Then, HA modification was performed as mentioned above, and Rhodamine B-labeled HA-MSN was obtained. A549-Luc-C8 cells were seeded 5×10^4 cells/well into 6-well plates and incubated for 24 h. After the incubation, the cells were treated with Rhodamine B-labeled HA-MSN (50 µg/mL) and incubation for 4 h. Then, washing process was performed three times with PBS, and the cell nuclei were stained with Hoechst after fixation with 2% paraformaldehyde. Finally, fluorescence images of the cells were obtained with fluorescent microscope.

2.5.3. Cytotoxicity Analysis (MTT Assay)

The cytotoxic effects of the NPs on cancerous and healthy lung cells were evaluated using the MTT assay as described by Mosmann (1983) [31]. Briefly, 1×10^4 cells/well were seeded into 96-well plates and incubated for 24 h to allow cell attachment. After incubation, the cells were treated with free CDDP, MSN, HA-MSN, MSN-CDDP, and HA-MSN-CDDP at various drug concentrations (200, 100, 20, 10, 2, and 1 µg/mL) and incubated for 48 h at 37 °C. Untreated cells served as the control group. Following treatment, 10 µL of MTT solution (5 mg/mL in PBS) was added to each well, and the plates were incubated for an additional 4 h to allow formazan crystal formation. The supernatant was then carefully removed, and 150 µL of DMSO was added to dissolve the formazan crystals. The optical density (OD) of each well was measured at 570 nm using a microplate reader (Synergy HT, BioTek Instruments, Winooski, VT, USA). Cell viability (%) was calculated using the following equation:

$$\text{Viable cells\%} = \frac{[(the\ absorbance\ of\ the\ treated\ cells) - (the\ absorbance\ of\ the\ blank)]}{[(the\ absorbance\ of\ the\ control) - (the\ absorbance\ of\ the\ blank)]} \times 100 \quad (2)$$

2.5.4. Apoptosis Analysis by Flow Cytometry

Flow cytometric analysis using the Annexin V-FITC/PI Apoptosis Detection Kit was performed to determine the apoptotic effects of free CDDP and nanoparticle formulations on A549-Luc-C8 cells. Briefly, 5×10^5 cells/well were seeded into 6-well plates and incubated for 24 h to allow cell attachment. The cells were then treated with free CDDP, MSN-CDDP, and HA-MSN-CDDP at their respective IC_{50} concentrations and incubated for 48 h at 37 °C. Following treatment, the cells were harvested, washed twice with cold PBS, and stained with Annexin V-FITC and propidium iodide (PI) in the dark at room temperature according to the manufacturer's protocol. Finally, the stained cells were analyzed by flow cytometry (BD Biosciences, Franklin Lakes, NJ, USA) to quantify the percentages of live, early apoptotic, late apoptotic, and necrotic cells.

2.5.5. Lactate Dehydrogenase (LDH) Cytotoxicity Assay

The cytotoxic effects of the NPs were further evaluated by measuring lactate dehydrogenase (LDH) release using a commercial LDH Cytotoxicity Assay Kit (Cayman Chemical Company 601170, Ann Arbor, MI, USA). LDH is a cytosolic enzyme released into the culture medium upon plasma membrane damage, and its activity serves as an indicator of cell necrosis. An increase in LDH activity in the culture supernatant corresponds to a higher degree of cell membrane damage. For the assay, PBMCs were seeded at a density of 1×10^6 cells/well in 48-well plates and incubated at 37 °C in a humidified atmosphere containing 5% CO_2 and 95% air. The cells were then treated with the NPs at their respective IC_{50} concentrations for 48 h. After incubation, 90 µL of the culture supernatant from each well (including negative control, positive control, and treatment groups) was transferred to a new plate. Subsequently, 10 µL of LDH assay reagent was added to each well, and the plate was incubated for 30 min at 37 °C. The absorbance was measured at 450 nm using a microplate reader (Synergy HT, BioTek Instruments, Winooski, VT, USA). Mitomycin-C was used as a positive control, as it induces maximal LDH release from damaged cells.

2.5.6. Total Oxidative Status (TOS) Assay

The total oxidant status of the cell culture medium was determined using a commercial TOS assay kit following the manufacturer's instructions. The assay is based on the oxidation of a ferrous ion–chelator complex to ferric ions by oxidants present in the sample. The resulting ferric ions form a colored complex with a chromogenic reagent, and the color intensity is proportional to the total oxidant concentration. For the experiment, PBMCs were treated with the NPs at their respective IC_{50} concentrations and incubated at 37 °C in a humidified atmosphere containing 5% CO_2 for 2 h. After incubation, 500 µL of Reagent 1 was mixed with 75 µL of each sample, and the absorbance was measured at 530 nm after 30 min. Subsequently, 15 µL of Reagent 2 was added to each well, and the absorbance was read again at 530 nm. A hydrogen peroxide (H_2O_2) standard was used to calibrate the assay, and TOS levels were expressed as micromoles of H_2O_2 equivalent per liter (µmol H_2O_2 equiv./L) [32].

2.5.7. Chromosome Aberration (CA) Assay

The CA assay for PBMCs was performed as described by Guler et al. (2023) [32]. PBMCs and the IC_{50} concentrations of free CDDP and the NPs were added to 6 mL of Chromosome Medium B and incubated for 72 h at 37 °C in a humidified atmosphere. Two hours before the end of the incubation period, 0.1 mL of colcemide solution was added to arrest cells at metaphase. Following incubation, the cells were harvested by centrifugation, and the pellet was treated with a hypotonic solution (0.075 M KCl) to swell the cells. The cell suspension was then re-incubated briefly and centrifuged again. The

resulting pellet was fixed using a methanol: acetic acid (3:1, *v*/*v*) solution, and this fixation step was repeated until the cell suspension became clear. A few drops of the fixed cell suspension were dropped onto clean, cold microscope slides and allowed to air-dry. The slides were then stained with Giemsa solution prepared in phosphate buffer (pH 6.8) and left to dry at room temperature. For cytogenetic evaluation, fifty well-spread metaphase plates were analyzed per sample under a light microscope to identify and record structural and numerical chromosomal aberrations.

2.5.8. Micronucleus (MN) Assay

PBMCs and the IC_{50} concentrations of free CDDP and the NPs were added to 7 mL of Chromosome Medium B containing 100 U/mL of penicillin, 100 µg/mL of streptomycin, and 0.5 mL of phytohemagglutinin, and the cell culture was incubated at 37 °C for 72 h. Cytochalasin B was added to the culture medium at 44 h of incubation. After the incubation, the culture medium was centrifuged at 900× *g* for 10 min, and the obtained lymphocyte cells were hypnotized by 0.075 M of cold potassium chloride for 30 min, and then cells were fixed with ice-cold methanol and acetic acid (3:1, *v*/*v*). The fixed cells were put directly on slides using Cytospin and stained with Giemsa solution. MN cells were counted under a light microscope. For all concentrations (duplicate cultures for each concentration), at least 1000 binucleated cells were counted for the formation of one, two, or more MN [32].

2.5.9. Salmonella Reverse Mutation Assay (Ames Test)

The mutagenicity potentials of free CDDP and the NPs were determined by the Ames test. For this purpose, TA98, TA100, TA1535 and TA1537 strains of *Salmonella typhimurium* were used [33]. Aroclor 1254 was used to induce rat liver S9, and it was used for metabolic activation (S9 mixture). Each experiment was performed in triplicate. Sodium azide was used as a positive control agent. Bacteria cultures in Xenometrix growth medium (PMM-GMOO, LOT: K05672P) were incubated at 37 °C for 12–14 h with shaking incubator at 100 rpm continuously. Subsequently, 100 µL of cultures and 100 µLs of these compounds (according to cisplatin concentration 50, 100 and 200 µg/mL) were added to melted top agar (2 mL) including histidine (0.5 mM) and biotin (0.5 mM). The tubes were shaken and then inoculated on the Minimal Glucose Agar (MGA) plates. The plates were incubated at 37 °C for 48 h. After incubation period, number of his + revertant colonies was counted.

2.5.10. Hemolysis Assay

Hemocompatibility of the NPs was analyzed with a hemolysis assay. This study was approved by Ege University, Local Ethical Committee of Animal Experiment (No. 2021-026). The blood samples were collected from rabbits into Li-heparinized tubes and centrifuged at 700× *g* for 10 min. After obtaining the pellet, it was washed with PBS and centrifuged again under the same conditions. Then, the pellet was resuspended with PBS pH 7.4. It was treated with different free CDDP and NPs concentrations in tubes. Also, 1% Triton X-100 was used as positive control. The tubes were incubated in a shaking water bath for 60 min at 37 °C and centrifuged again under the same conditions. To determine the released hemoglobin amount, the supernatant was measured at 540 nm by spectrophotometer. Hemolysis percentage was calculated using the following equation [32]:

$$Percent\ hemolysis\ (\%) = \frac{\text{Sample absorbance} - \text{Negative control absorbance}}{\text{Positive control absorbance} - \text{Negative control absorbance}} \times 100 \quad (3)$$

2.6. In Vivo Assays

2.6.1. Animals

The experimental procedures were approved by the Ege University, Local Ethical Committee of Animal Experiment (approval date: 27 February 2022 and approval No. 2021-026). All procedures were conducted in accordance with the ARRIVE Guideline 2.0 [34]. Healthy male and female Balb/c nude mice (weighing 20–25 g) were obtained from Izmir Biomedicine and Genome Center (Izmir-Türkiye). The animals were housed in groups of six per cage in stainless steel cages under controlled environmental conditions (22.0 ± 2.0 °C, relative humidity 45–65%) with a 12 h light/dark cycle. Throughout this study, the animals were fed with standard laboratory feed and water, ad libitum. They were observed daily, and body weights were recorded before and during the study period.

2.6.2. Experimental Lung Cancer Model

Subcutaneous xenograft lung tumors were established by injecting 1×10^7 A549-Luc-C8 cells suspended in PBS into the right flank of each mouse [35]. Tumor growth and localization were monitored using an in vivo imaging system (IVIS Spectrum, PerkinElmer Inc., Waltham, MA, USA) with the IVISense™ Vascular 680 fluorescent probe. When the tumor volume reached approximately 50 mm^3, it was designated as day 0, and treatment was initiated. The mice were randomly divided into four groups (n = 6 per group): Saline (SF) as a control group, Free CDDP (10 mg/kg), MSN-CDDP (equivalent to 10 mg/kg cisplatin), and HA-MSN-CDDP (equivalent to 10 mg/kg cisplatin). Treatments were administered intraperitoneally (ip) twice per week for 14 days. Throughout the treatment period, body weights and tumor sizes were monitored regularly using the IVIS system to assess therapeutic efficacy. On day 14, the mice were sacrificed, and tumors and major organs were excised for further histopathological and biochemical analyses [36].

2.6.3. Biochemical Analyses

After the treatment, on 14th day the blood was taken from mice hearts after ketamine + xylazine overdose anesthesia. Then, the serum was obtained, and the biochemical analysis was established with Fujifilm FUJI DRI-CHEM NX500V IC device (Fuji, Tokyo, Japan) with Comprehensive S Panel kit. The dissected tissues were taken out from −80 °C, weighed, and homogenized in phosphate buffer (pH 7.4) including PMSF and DTT. A 3 mL buffer was used per 1 g of a tissue sample. Tissue homogenates were centrifuged at 15,000× *g* at 4 °C for 15 min, and the supernatant was used as an enzyme source. Each sample was studied with three replicates.

Total protein content of tissue samples was determined using the Bradford assay [37]. Superoxide dismutase (SOD; EC 1.15.1.1) activity was measured according to the method described by Ewing and Janero (1995), which is based on the rate of nitroblue tetrazolium (NBT) reduction. SOD activity was expressed as the concentration required to inhibit the initial rate of NBT reduction by 50% (IC_{50}) [38]. Absorbance was measured at 560 nm using a microplate reader (BioTek Epoch 2), and results were expressed as U/mg protein. Catalase (CAT; EC 1.11.1.6) activity was determined according to Beers and Sizer (1951) [39]. The reaction relies on the decomposition of H_2O_2, and absorbance was recorded spectrophotometrically at 240 nm using quartz cuvettes [39]. Lipid peroxidation was evaluated by measuring thiobarbituric acid reactive substances (TBARSs), which are products of lipid peroxidation. Samples reacted with thiobarbituric acid (TBA), and absorbance was measured at 532 nm and 600 nm using a Perkin Elmer UV/Vis Spectrometer (Lambda 25) [40]. TBARS concentration was calculated using an extinction coefficient (ε) of 155 mM^{-1} cm^{-1}.

2.6.4. Histological and Immunohistochemical (IHC) Assessment

Excised tissues (lung, liver and kidney) were collected in Falcon tubes and washed with PBS. The tissues were then fixed in 10% buffered formalin overnight. After fixation, samples were dehydrated through a graded ethanol series (70%, 80%, 96%, and 100%) and air-dried. Tissues were subsequently cleared in xylene for 30 min until transparent and embedded in paraffin. The paraffin blocks were sectioned at 5 µm thickness, mounted onto glass slides, and dried overnight at 37 °C. Sections were then deparaffinized, rehydrated, and stained with hematoxylin and eosin (H&E). Histological evaluation was performed using a light microscope (Olympus BX51, Tokyo, Japan), and images were captured with an Olympus C-5050 digital camera.

For IHC, tissue sections were first incubated with 3% H_2O_2 for 10 min to quench endogenous peroxidase activity, followed by blocking with Super Block for 20 min at room temperature. Sections were then incubated overnight at 4 °C in a humidified chamber with a primary antibody against Ki67 (diluted 1:100). The following day, slides were incubated sequentially with a biotinylated secondary antibody and streptavidin-HRP, each for 30 min. Immunoreactivity was visualized using a DAB chromogen substrate (UltraTek HRP Anti-Polyvalent, ScyTec Inc., Greenwood Village, CO, USA), and counterstaining was performed with Mayer's hematoxylin (Sigma-Aldrich). Stained sections were examined under a light microscope, and representative images were captured for analysis.

2.7. Statistical Analyses

Statistical analysis of the in vitro data was performed using GraphPad Prism version 9. Comparisons among groups were performed using one-way analysis of variance (ANOVA) followed by Duncan's multiple comparison test. For the in vivo studies, data were analyzed using SPSS software version 25.0 (IBM Corp., Armonk, NY, USA). The normality of the data distribution was assessed using the Kolmogorov–Smirnov test. Comparisons among groups were performed using ANOVA followed by the least significant difference (LSD) post hoc test. Data are presented as mean ± standard deviation (SD), and a p value of ≤ 0.05 was considered statistically significant.

3. Results and Discussion

Conventional chemotherapeutic agents often suffer from poor tumor specificity, resulting in low bioavailability and severe off-target toxicity. MSNs have emerged as promising drug delivery systems for cancer therapy due to their biocompatibility, biodegradability, high drug-loading capacity, and easily modifiable surface chemistry [7]. HA modification, in particular, enables selective targeting of CD44-overexpressing cancer cells, making it an effective strategy for developing chemotherapeutic-loaded NPs [12]. In this study, high-molecular-weight HA-modified, cisplatin-loaded MSNs (HA-MSN-CDDP) were successfully synthesized to target CD44-overexpressing lung adenocarcinoma cells, thereby enhancing therapeutic efficacy while minimizing systemic toxicity of cisplatin.

3.1. Characterization of NPs

The chemical structure and surface functionalization of the NPs were confirmed by FTIR spectroscopy (Figure 1a). For pure silica, a broad absorption band in the range of 3400–3600 cm^{-1} corresponded to the ν(O–H) stretching vibration, attributed to hydrogen-bonded silanol groups. A weak peak observed at 1634 cm^{-1} was ascribed to δ(O–H) bending vibration. The strong band at 1000–1150 cm^{-1} (centered around 1079 cm^{-1}) represented the ν(Si–O–Si) asymmetric stretching of the silica network. The weak shoulder at 961.5 cm^{-1} was associated with ν(Si–O) stretching of non-condensed silanol groups (Si–OH), while peaks at approximately 799 cm^{-1} and 467 cm^{-1} corresponded to symmetric

stretching and bending vibrations of Si–O–Si, respectively. Successful surface silanolization was confirmed in the FTIR spectrum of MSN–NH_2. The appearance of a peak at 3610 cm^{-1} indicated the presence of amine (–NH_2) groups, whereas peaks at 2927 cm^{-1} and 2856 cm^{-1} corresponded to the asymmetric and symmetric stretching of –CH_2 groups from the propyl chain introduced by APTES. The three characteristic Si–O–Si peaks at 1060 cm^{-1} (broad), 797 cm^{-1}, and 457 cm^{-1} were due to asymmetric and symmetric stretching and bending of Si-O-Si vibrations from the silica network, respectively. The decreased intensities of the bands at 1627 cm^{-1} and 961 cm^{-1} further supported the grafting of amino groups onto surface silanol sites [41,42]. Following HA conjugation, the characteristic –NH_2 peaks at 3600 cm^{-1} and 1530 cm^{-1} disappeared, indicating successful coupling of HA to MSN–NH_2. Additionally, the appearance of a new band at 1640 cm^{-1} corresponding to the C=O stretching vibration of amide bonds confirmed the formation of HA–MSN through EDC/NHS-mediated amidation [43,44]. These results collectively verified the successful surface modification of MSNs with HA. An amide bond was formed between amine groups of MSNs and carboxyl groups of HA.

It is crucial that the NP administered in the drug delivery system reaches the target area to maximize the benefit from the medication. Therefore, to ensure effective treatment, the administered NP should not be rapidly eliminated from the body and remain in circulation for an extended period [45]. The biodistribution, pharmacokinetics, and toxicity of NPs in biological systems largely depend on their physicochemical characteristics, particularly particle size and surface charge [46,47]. DLS analysis revealed that the average sizes of MSN, HA-MSN, MSN-CDDP, and HA-MSN-CDDP were 137.4 ± 0.7 nm, 279.7 ± 2.8 nm, 370.7 ± 10.5 nm, and 324.8 ± 19.6 nm, respectively. It is known that HA is a highly hydrophilic biopolymer, and DLS measurement is based on the Brownian motion of NPs. Therefore, the size of NPs in DLS measurement has escalated after HA modification [21,24,44]. As expected, HA modification increased the hydrodynamic diameter of the NPs due to the high molecular weight and hydrophilic nature of the HA. PdI values of the NPs were obtained, and they were nearly monodispersed. The measured zeta potentials of MSN, MSN–NH_2, HA-MSN, MSN-CDDP, and HA-MSN-CDDP were −28.9 ± 5.4 mV, +22.9 ± 3.7 mV, −20.4 ± 2.3 mV, −25.7 ± 0.8 mV, and −16.2 ± 1.1 mV, respectively (Figure 1b,d; Table 1). The positive surface charge of MSN–NH_2 confirmed successful amine functionalization, while the subsequent decrease to a negative charge following HA conjugation resulted from the carboxyl groups present in HA [14,44]. Differences between DLS and electron microscopy size measurements are attributed to the techniques used. DLS measures the hydrodynamic diameter, which includes the solvation layer surrounding the particles in suspension, whereas SEM and TEM measure the solid particle core [48]. SEM and TEM images confirmed that all NPs were spherical, with well-ordered mesoporous structures and narrow size distributions (Figure 1c). The average diameters determined by electron microscopy for MSN, HA-MSN, MSN-CDDP, and HA-MSN-CDDP were monodispersed and 53.6 ± 3.6 nm, 60.6 ± 3.0 nm, 63.6 ± 6.1 nm, and 52.7 ± 2.8 nm, respectively. The size, charge and shape are related to distribution and clearance of NPs in the biological system. The <200 nm NPs have a long circulation time in the body. In addition, 20–200 nm NPs have high bioaccumulation in tumor sites to overcome rapid elimination. Positive-charged NPs can induce an immune response. Therefore, negative and neutral charges offer an advantage to NPs in terms of biomedical applications due to escape degradation by phagocytic cells, and they are better candidates particularly as drug carriers. Between −30 and 30 mV surface charge provides NPs stabilization and prevents aggregation. Also, spherical shape NPs have biocompatible properties and are easily internalized by cells [3,46,49]. Hydrophobic NPs are rapidly eliminated from the body by phagocytes. HA has negative charge and is a highly hydrophilic biopolymer. MSN

has hydrophilic properties and excellent colloidal dispersity after conjugation with HA. In this way, the researchers have solved the agglomeration problem of MSNs, increasing the circulation time and the chance of reaching the tumor [41]. Taken together, HA-MSN-CDDP has a good drug candidate for anticancer therapy owing to its determined physicochemical properties. CDDP was loaded into MSN/HA-MSN pores. Non-covalent interaction, especially adsorption, occurred between CDDP and MSN/HA-MSN due to the mesoporous structure of MSNs, which provides the high loading drug capacity. Considering the drug loading content, the following was determined: 348.4 mg cisplatin/g MSN-CDDP and 345.6 mg cisplatin/g HA-MSN-CDDP.

3.2. In Vitro Antitumor Efficiency and Toxicity

3.2.1. Drug Release Profiles

The purpose of smart drug delivery systems is to enhance the bioavailability of anticancer agents by preventing their premature release, enabling targeted accumulation at the tumor site, and ensuring controlled drug release under physiological conditions [45]. To evaluate the release behavior of cisplatin, drug release studies were conducted at pH 7.4 and pH 5.5, which simulate the physiological pH of blood and the acidic microenvironment of tumors, respectively, at 37 °C, corresponding to human body temperature. As shown in Figure 2a,b, the cumulative release profiles of CDDP followed the order free CDDP > MSN-CDDP > HA-MSN-CDDP at both pH conditions. The slower release observed from HA-MSN-CDDP demonstrates that surface modification with HA not only prolongs systemic circulation but also provides sustained and controlled drug release. Similar controlled-release behavior has been reported for HA-modified NPs encapsulating various chemotherapeutics, including CDDP [20,21,50,51].

3.2.2. Confirmation of Cellular Uptake

Cellular internalization of the nanoparticles was further confirmed using Rhodamine B-labeled HA-MSN. The nuclei of A549-Luc-C8 cells were counterstained with Hoechst dye (blue), while Rhodamine B fluorescence (red) indicated the localization of the NPs. Although the red fluorescence signals were not contained in the control group (Figure 2c), as shown in Figure 2d, the red fluorescence signals were distributed in the perinuclear region, confirming the successful uptake of HA-MSN by A549-Luc-C8 cells. HA modification provides to increase in NPs uptake thanks to the CD44-specific affinity of HA. It is known that cellular uptake of HA-modified NPs is realized by receptor-mediated endocytosis. In parallel with our results, HA has improved cellular uptake of chemotherapeutic-loaded NPs into CD44 overexpressing cells by endocytosis [14,17,52].

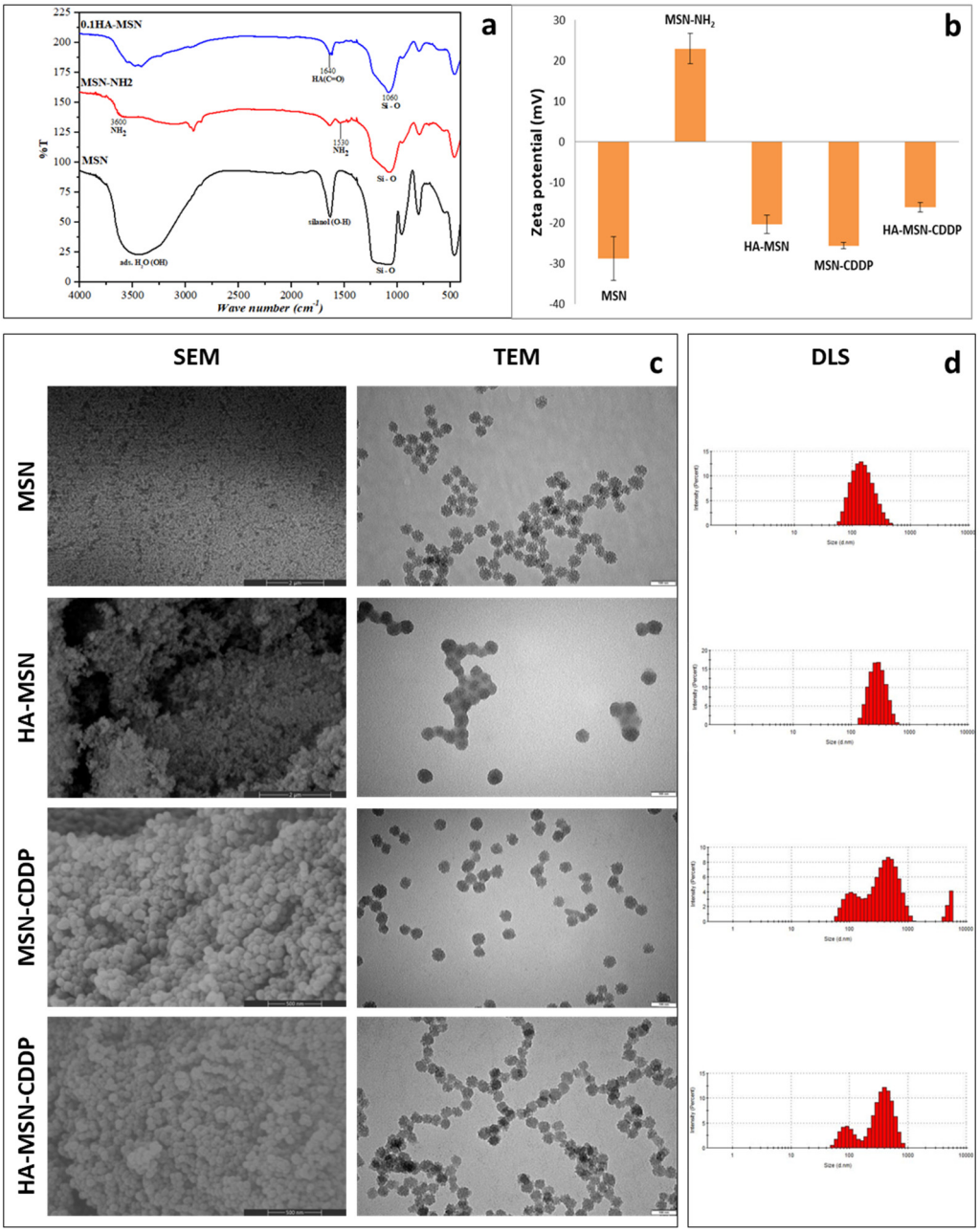

Figure 1. (**a**) Fourier transform infrared (FTIR) spectra for MSN (black), MSN-NH_2 (red) and HA-MSN (blue). (**b**) Zeta potential of the NPs. (**c**) Scanning electron microscopy (SEM, bar scale 500 nm) and Transmission electron microscopy (TEM, bar scale 100 nm) images of the MSN, HA-MSN, MSN-CDDP and HA-MSN-CDDP. (**d**) Dynamic light scattering (DLS) size distributions of MSN, HA-MSN, MSN-CDDP and HA-MSN-CDDP.

Table 1. Size, zeta potential and PdI values of the NPs. Data is presented as mean ± SD.

Groups	Size (nm)	Surface Potential (mV)	PdI
MSN	137.4 ± 0.7	−28.9 ± 5.4	0.146
HA-MSN	279.7 ± 2.8	−20.4 ± 2.3	0.121
MSN-CDDP	370.7 ± 10.5	−25.7 ± 0.8	0.406
HA-MSN-CDDP	324.8 ± 19.6	−16.2 ± 1.1	0.372

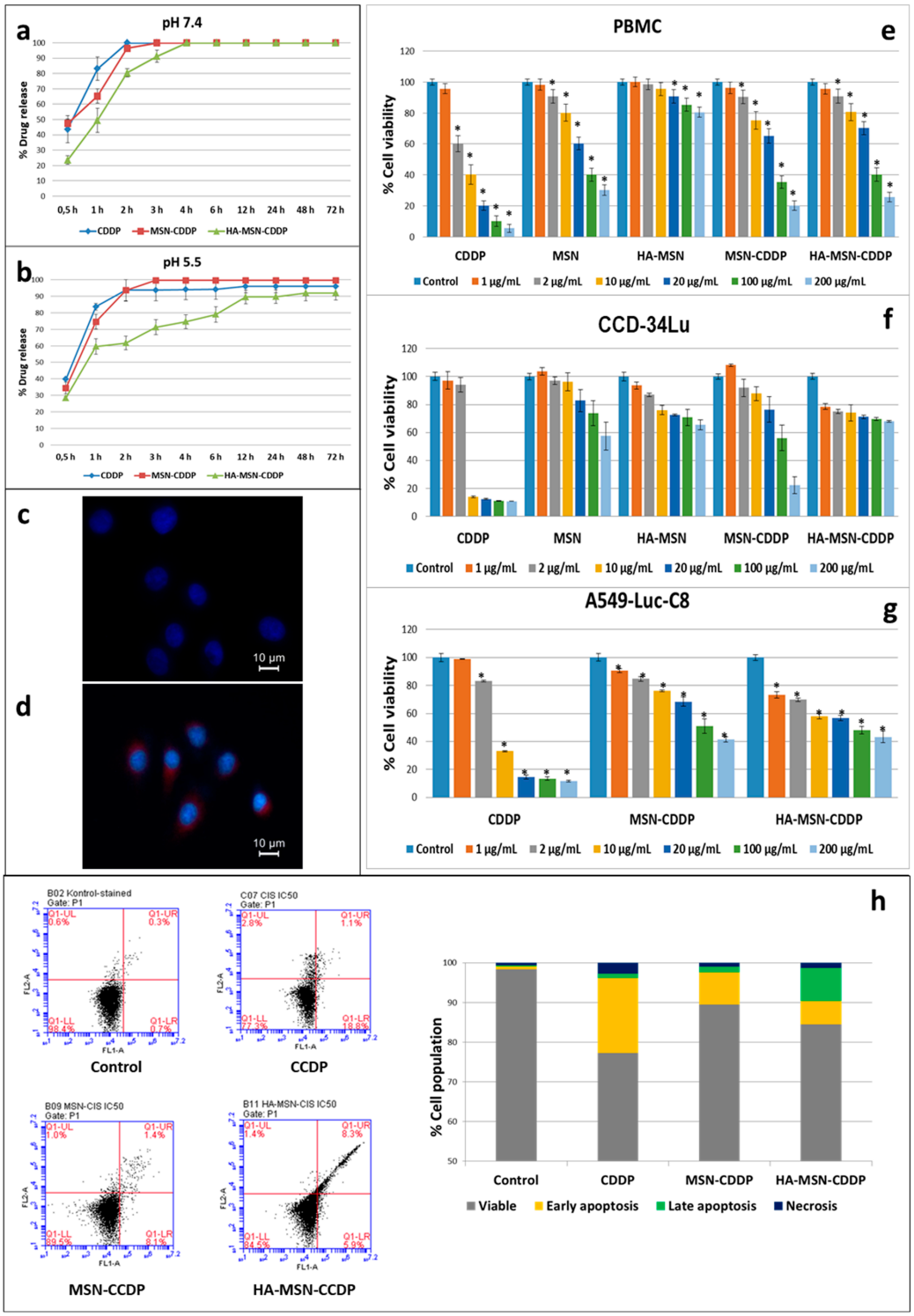

Figure 2. In vitro drug releases of Cisplatin from CDDP, MSN-CDDP and HA-MSN-CDDP in phosphate-buffered saline (PBS): (**a**) pH 7.4, (**b**) pH 5.5. (**c**) Fluorescence microscope image of cellular uptake of control group (scale bar 10 µm) (**d**) and Rhodamine B-labeled HA-MSN by A549-Luc-C8 cells (scale bar 10 µm). (**e**) PBMC, (**f**) CCD-34Lu, (**g**) A549-Luc-C8 cell viabilities after 48 h of treatment to 1, 2, 10, 20, 100 and 200 µg/mL (according to Cisplatin concentration) of CDDP, MSN, HA-MSN, MSN-CDDP and HA-MSN-CDDP. (**h**) Apoptosis rate after CDDP, MSN-CDDP and HA-MSN-CDDP treatment (according to IC_{50} concentrations on A549-Luc-C8 cells). Data is presented as mean± SD from three repeats and three independent experiments. * Statistically significant difference compared to the control group ($p < 0.05$).

3.2.3. Cytotoxic, Apoptotic and Oxidative Stress Effects of NPs

In drug delivery applications, NPs can interact with cells and induce cytotoxic and/or genotoxic effects, often associated with oxidative stress generation. The extent of these toxic responses depends largely on the physicochemical characteristics of the NPs, including size, surface charge, and composition [7,49]. The anticancer activities of free CDDP, MSN-CDDP, and HA-MSN-CDDP were evaluated in A549-Luc-C8 lung adenocarcinoma cells. Free CDDP exhibited a strong cytotoxic effect against the cells with an IC_{50} value of 6.73 ± 0.29 μg/mL. In contrast, the IC_{50} values of MSN-CDDP and HA-MSN-CDDP were 86.03 ± 7.48 μg/mL and 42.03 ± 8.63 μg/mL, respectively, indicating that HA-MSN-CDDP maintained significant anticancer activity while reducing toxicity compared to free CDDP (Figure 2e–g; Table 2). On the other hand, CDDP has a very serious cytotoxic effect on healthy CCD-34Lu and PBMC cells. The healthy cell viabilities for all applied concentrations of HA-MSN were over 50%. High concentrations of MSN-CDDP exhibited cytotoxic activity, with an IC50 value of 88.75 ± 29.1 μg/mL and 65 ± 1.52 μg/mL on CCD-34Lu and PBMC cells, respectively. However, HA-MSN-CDDP has a high percentage of cell viability on CCD-34Lu cells even at the highest applied concentration of 200 μg/mL. In addition, the IC50 value of HA-MSN-CDDP on PBMC cells was 76 ± 2.25 μg/mL. CDDP induces apoptosis by interacting with DNA and destroying cancer cells. However, it also causes an unwanted cell killing mechanism, which is necrosis [53]. In this study, CDDP induced not only apoptosis but also necrosis for A549-Luc-C8 cells. Early apoptosis was identified as the main mechanism of action. Treatment with HA-MSN-CDDP led to an increased rate of late apoptosis while reducing necrosis, likely due to HA–CD44 interactions and the controlled release of CDDP. Also, HA-MSN-CDDP has stronger apoptotic effect than MSN-CDDP (Figure 2h).

Table 2. Cytotoxicity of CDDP and the nanoparticles on the cell lines.

Groups	IC_{50} (μg/mL) (Mean ± SD)		
	A549-Luc-C8	**CCD-34Lu**	**PBMC**
CDDP	6.73 ± 0.29	5.45 ± 0.19	7.5 ± 0.82
MSN	-	>200	121.3 ± 3.42
HA-MSN	-	>200	>200
MSN-CDDP	86.03 ± 7.48	88.75 ± 29.1	65 ± 1.52
HA-MSN-CDDP	42.03 ± 8.63	>200	76 ± 2.25

HA-MSN-CDDP was effectively uptaken by CD44-overexpressing A549-Luc-C8 cells. In parallel with our results, apoptosis induction of CDDP in CD44 overexpressing MCF7, U87 and MDA-MB-231 cells has increased thanks to HA [24,51,53]. In parallel with the MTT results, the LDH activity of HA-MSN-CDDP in PBMC cells was quite lower (4.28-fold) than CDDP (Figure 3a). TOS activity results showed that MSN-CDDP and HA-MSN-CDDP have 1.9-fold and 2.7-fold decreases compared to CDDP, respectively (Figure 3b). Although CDDP has a drastic anticancer effect on the lung cancer cells compared to the CDDP-loaded NPs, it has caused unwanted cytotoxic activity on the healthy cells. HA-MSN-CDDP has better anticancer activity and is safer than MSN-CDDP thanks to HA modification. HA modification of HA-MSN-CDDP provides negative surface charge, hydrophilicity, stability in medium/biological system, targeting ability to CD44 and decreasing non-specific toxicity, and these properties make it a better drug candidate. Likewise, HA modification reduces cytotoxicity on different healthy cells of drug delivery systems thanks to CD44-specific interaction [18,19,43,50,53,54].

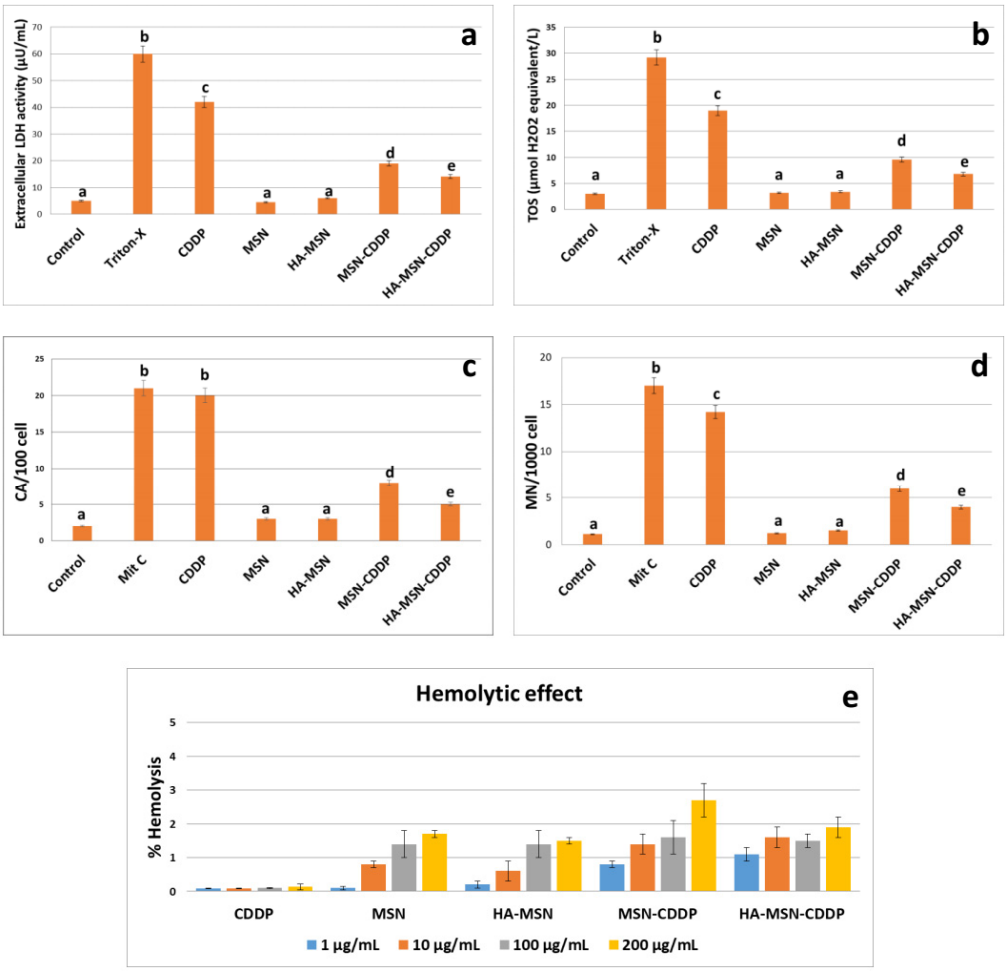

Figure 3. (**a**) Lactate Dehydrogenase (LDH) release levels in the cells exposed to IC_{50} concentrations of CDDP, MSN, HA-MSN, MSN-CDDP and HA-MSN-CDDP after 48 h. (**b**) Total oxidative stress (TOS) levels in the cells after CDDP, MSN, HA-MSN, MSN-CDDP and HA-MSN-CDDP treatment at IC_{50} concentrations. (**c**) Chromosomal aberration (CA) ratio in PBMCs after exposure to CDDP, MSN, HA-MSN, MSN-CDDP and HA-MSN-CDDP for 72 h. (**d**) Micronucleus (MN) ratio in PBMCs after exposure to IC_{50} concentrations of CDDP, MSN, HA-MSN, MSN-CDDP and HA-MSN-CDDP for 72 h. (**e**) Hemolytic effect after CDDP, MSN, HA-MSN, MSN-CDDP and HA-MSN-CDDP treatment (1, 10, 100 and 200 µg/mL according to Cisplatin). All data is presented as mean ± SD from three repeats and three independent experiments. Different letters (a, b, c, d, and e) in the column indicate statistical differences between the groups ($p < 0.05$).

3.2.4. Genotoxic Effect

Genotoxic effect of NPs occurs in two ways: directly interacting with DNA or inducing ROS formation [47]. Also, CDDP causes mutagenicity and carcinogenicity. In the AMES test, CDDP has led to mutagenic effects on TA98, TA100 and TA102 strains of *S. typhimurium* [55]. Our results showed that CDDP had a significant mutagenic effect on TA98, TA100, TA1535 and TA1537 strains of *S. typhimurium*. MSN-CDDP and HA-MSN-CDDP decreased the effect, and the mutagenicity was concentration-dependent (Table 3). In addition, in the CA test, MSN-CDDP and HA-MSN-CDDP showed 2.5-fold and 4-fold decreasing chromosome aberration compared to CDDP, respectively, and in the MN test, MSN-CDDP and HA-MSN-CDDP showed 2.36-fold and 3.55-fold decreasing micronucleus formation compared to CDDP, respectively (Figure 3c,d). In parallel with our results, genotoxicity of CDDP has decreased via NP administration [56].

Table 3. His+ revertant colony numbers after treatment.

Groups	Conc. (μg/mL)	His⁺ Revertant Colony Numbers (Mean ± SD)							
		TA 98		TA 100		TA 1535		TA 1537	
		−S9	+S9	−S9	+S9	−S9	+S9	−S9	+S9
NC	100 μL	13 ± 1	15 ± 5	110 ± 4	119 ± 9	12 ± 2	28 ± 2	6 ± 1	9 ± 3
CDDP	200	1050 ± 212	1043 ± 106	410 ± 42	623 ± 174	61 ± 5	92 ± 26	4 ± 1	120 ± 59
	100	88 ± 6	69 ± 13	211 ± 23	476 ± 175	3 ± 2	5 ± 1	4 ± 1	9 ± 1
	50	63 ± 27	59 ± 34	153 ± 10	109 ± 23	8 ± 1	6 ± 6	5 ± 3	7 ± 1
MSN	200	13 ± 1	14 ± 1	184 ± 36	169 ± 5	35 ± 11	26 ± 6	9 ± 2	9 ± 2
	100	18 ± 4	15 ± 4	176 ± 17	145 ± 2	42 ± 29	14 ± 4	8 ± 4	5 ± 2
	50	11 ± 2	22 ± 4	119 ± 69	102 ± 2	30 ± 5	43 ± 17	8 ± 4	5 ± 2
HA-MSN	200	20 ± 3	20 ± 1	205 ± 29	210 ± 2	22 ± 7	23 ± 1	5 ± 2	2 ± 1
	100	16 ± 1	12 ± 3	192 ± 6	242 ± 53	20 ± 6	27 ± 4	8 ± 1	7 ± 7
	50	16 ± 4	15 ± 10	188 ± 46	201 ± 4	20 ± 1	16 ± 6	4 ± 4	5 ± 1
MSN-CDDP	200	17 ± 5	20 ± 10	171 ± 8	330 ± 71	27 ± 2	29 ± 2	6 ± 1	2 ± 1
	100	10 ± 6	19 ± 4	138 ± 9	210 ± 6	11 ± 3	8 ± 1	8 ± 2	8 ± 1
	50	17 ± 1	179 ± 19	124 ± 20	192 ± 20	11 ± 4	16 ± 3	6 ± 1	8 ± 1
HA-MSN-CDDP	200	24 ± 4	2 ± 1	216 ± 6	204 ± 11	21 ± 9	30 ± 4	7 ± 4	6 ± 3
	100	16 ± 1	16 ± 6	172 ± 5	148 ± 17	18 ± 4	32 ± 6	5 ± 2	7 ± 4
	50	9 ± 4	24 ± 13	147 ± 24	164 ± 34	6 ± 1	16 ± 9	5 ± 3	5 ± 4
PC	100	1600 ± 42	1720 ± 55	1560 ± 57	1410 ± 42	1480 ± 113	1200 ± 113	3360 ± 54	485 ± 35

NC: distilled water, PC: sodium azide.

3.2.5. Hemolytic Effect

Since cisplatin is administered intravenously, it is crucial that the designed NP drug delivery system exhibits good hemocompatibility. The hemolytic effect of MSNs depends on various factors such as size, surface charge, concentration and pore structure. An MSN has a lower hemolytic effect than non-porous silica NPs [57,58]. According to ISO/TR 7406, NPs exhibiting a hemolytic rate below 5% are considered hemocompatible. As shown in Figure 3e both free CDDP and CDDP-loaded nanoparticles demonstrated hemolysis rates within this acceptable range, confirming their hemocompatibility. Notably, HA-MSN-CDDP exhibited a lower hemolytic effect compared to MSN-CDDP, indicating that HA surface modification further improved blood compatibility. The enhanced hemocompatibility of HA-MSN-CDDP is attributed to the shielding of silanol groups on the MSN surface, which are otherwise capable of interacting with and disrupting erythrocyte membranes, potentially causing hemolysis [58]. The introduction of HA provided a negatively charged, hydrophilic, and biocompatible surface, effectively reducing erythrocyte membrane interactions and improving systemic safety [17,22,51].

3.3. In Vivo Antitumor and Toxicity Efficiency

3.3.1. Antitumor Efficacy in Xenograft Lung Cancer Mouse Model

The therapeutic efficacy of free CDDP and CDDP-loaded NPs was evaluated using a xenograft lung adenocarcinoma mouse model (Figure 4; Table 4). The control group (SF) showed no inhibition of tumor growth. Free CDDP treatment resulted in moderate tumor suppression compared to the control group. Although MSN-CDDP lacks an active tumor-targeting mechanism, it produced a greater reduction in tumor growth than free CDDP. Among all treatment groups, HA-MSN-CDDP demonstrated the most potent antitumor activity, leading to a significant reduction in tumor volume compared to CDDP and MSN-CDDP groups. While mice treated with CDDP exhibited noticeable body weight loss, no significant changes in body weight were observed in any of the NP-treated groups (Table 5). Likewise, unfortunately, tumor volume has increased through free CDDP treatment [36,51,53]. Also, free CDDP treatment has not prevented animal death [24,36]. In contrast, HA-MSN-CDDP significantly prevented body weight loss and suppressed tumor growth, confirming its superior therapeutic efficacy. Organ and relative organ weights of experimental groups are presented in Tables 6 and 7, further supporting the systemic safety

of HA-MSN-CDDP. In parallel with our results, different chemotherapeutic-loaded NPs have effective cancer treatment while maintaining animal weight stability and survival thanks to HA modification in breast, colon, and lung cancer [16,52,54,59–61]. The enhanced efficacy is primarily attributed to HA-mediated CD44 receptor targeting, which promotes selective tumor accumulation and internalization. Consequently, HA-MSN-CDDP achieved higher therapeutic efficiency while minimizing off-target toxicity, thereby improving the overall survival rate of tumor-bearing mice.

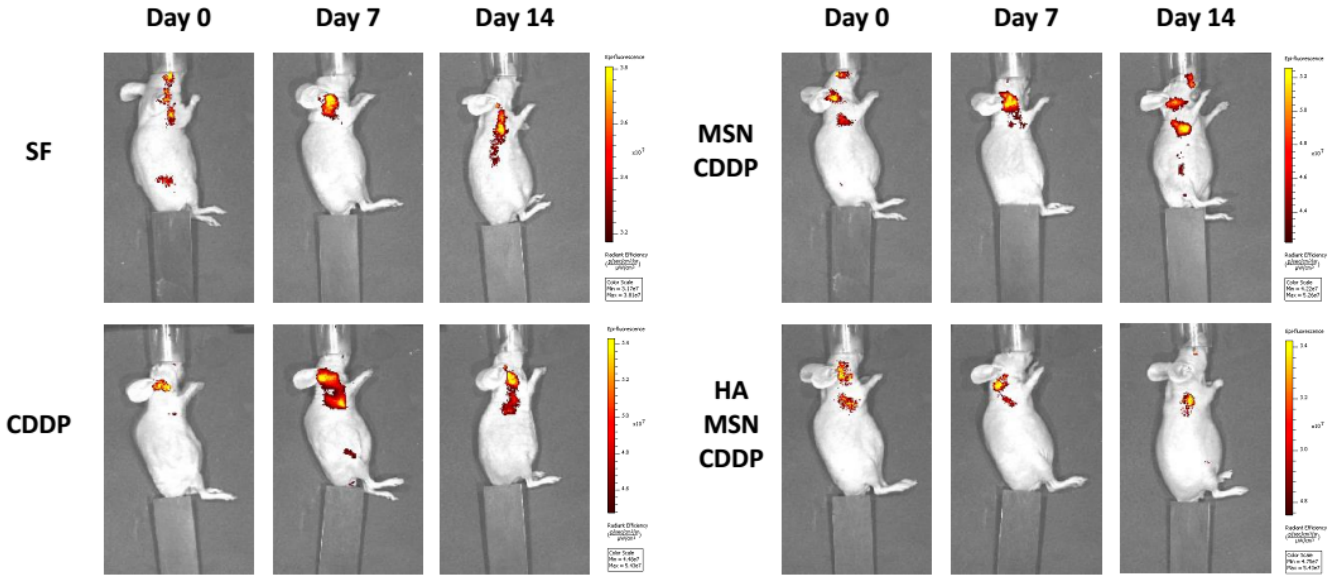

Figure 4. In vivo imaging of tumors in experimental animal groups at day 0, 7 and 14 by IVIS spectrum (excitation = 640 nm and emission = 700 nm).

Table 4. The region of interest (ROI) values of mice in experimental groups.

Treatment Groups	(Total ROI Values ± SD) × 10^8			ROI Value Changes (%) from Day 0 to Day 14
	Day 0	Day 7	Day 14	
Control (SF)	1.340 ± 0.109	2.791 ± 0.086	3.282 ± 0.363	245
CDDP	1.157 ± 0.319	3.079 ± 0.851	2.239 ± 0.085	93
MSN-CDDP	1.314 ± 0.601	3.150 ± 1.008	2.059 ± 0.770	57
HA-MSN-CDDP	1.269 ± 0.335	1.164 ± 0.337	0.845 ± 0.057	−33

Table 5. Total body weight values of animals in experimental groups starting from day 0 to 28, where tumor injection on day 14 is regarded as day 0 for the treatment.

Treatment Groups	Total Body Weights (Gram) (Mean ± SD)				
	Day 0	Day 7	Day 14 (Day 0)	Day 21 (Day 7)	Day 28 (Day 14)
Control (SF)	24.73 ± 3.72	24.26 ± 2.41	21.96 ± 1.36	22.24 ± 1.35	21.49 ± 1.84
CDDP	24.16 ± 2.88	24.60 ± 3.24	22.25 ± 2.79	21.01 ± 1.86	19.80 ± 1.35
MSN-CDDP	22.90 ± 2.87	23.20 ± 2.77	24.41 ± 3.06	24.49 ± 3.99	23.99 ± 3.51
HA-MSN-CDDP	21.09 ± 2.39	21.10 ± 3.85	22.67 ± 2.65	23.23 ± 3.26	23.03 ± 3.09
F	0.487	0.378	0.198	0.478	1.337
P	0.700	0.772	0.895	0.706	0.329

Table 6. Organ weights of mice in experimental groups at the end of this study.

Treatment Groups	Organ Weights (Gram) (Mean ± SD)				
	Heart	Brain	Lung	Liver	Kidney
Control (SF)	0.14 ± 0.026	0.27 ± 0.021 #	0.20 ± 0.078 #	1.35 ± 0.19	0.35 ± 0.011 #
CDDP	0.14 ± 0.017	0.21 ± 0.008 *	0.14 ± 0.022 *	1.02 ± 0.16	0.22 ± 0.011 *
MSN-CDDP	0.14 ± 0.030	0.28 ± 0.006 #	0.21 ± 0.036 #	1.49 ± 0.40	0.45 ± 0.080 #
HA-MSN-CDDP	0.15 ± 0.025	0.27 ± 0.015 #	0.17 ± 0.021	1.43 ± 0.28	0.42 ± 0.064 #
F	0.130	19.984	0.637	2.135	4.003
P	0.939	0.000	0.612	0.174	0.050

* Statistically significant difference compared to the control group ($p < 0.05$). # Statistically significant difference compared to the CDDP group ($p < 0.05$).

Table 7. Relative organ weights of mice in experimental groups at the end of this study.

Treatment Groups	Relative Organ Weights (Gram) (Mean ± SD)				
	Heart	Brain	Lung	Liver	Kidney
Control (SF)	0.0065 ± 0.0009 #	0.0127 ± 0.0010	0.0095 ± 0.0062	0.063 ± 0.0017	0.016 ± 0.0008 #
CDDP	0.0079 ± 0.0005 *	0.0118 ± 0.0014	0.0079 ± 0.0010	0.057 ± 0.0017	0.012 ± 0.0007 *
MSN-CDDP	0.0059 ± 0.0007 #	0.0124 ± 0.0035	0.0089 ± 0.0010	0.062 ± 0.0030	0.019 ± 0.0007 #
HA-MSN-CDDP	0.0066 ± 0.0010 #	0.0125 ± 0.0023	0.0076 ± 0.0017	0.063 ± 0.0047	0.018 ± 0.0006 #
F	4.090	0.093	0.204	2.458	27.624
P	0.049	0.962	0.891	0.138	0.000

* Statistically significant difference compared to the control group ($p < 0.05$). # Statistically significant difference compared to the CDDP group ($p < 0.05$).

3.3.2. Biochemical Evaluation

The biochemical parameters measured after treatment are summarized in Table 8. It is known that values of biochemical parameters are wide range in mice. Total protein (TP) and albumin (ALB) are important indicators of general health status and liver function. In the present study, TP and ALB levels remained within the normal reference range [62] across all experimental groups, indicating the absence of hepatic dysfunction. Because the kidneys are the primary route of cisplatin excretion, nephrotoxicity is a common adverse effect of platinum-based chemotherapeutics. Therefore, BUN and CRE levels were assessed in all groups, as they are key markers of renal function, and renal tissues are particularly vulnerable to CDDP-induced damage due to drug accumulation [26,63]. Consistent with this, animals receiving cisplatin alone displayed elevated BUN and CRE levels, confirming nephrotoxicity. In contrast, these values in the HA-MSN-CDDP-treated group remained within the normal reference range [62], demonstrating that HA-MSN-CDDP effectively attenuates cisplatin-induced renal toxicity.

The antioxidant defense system plays a critical role in maintaining cellular homeostasis by neutralizing reactive oxygen species (ROS). Free CDDP is known to induce ROS overproduction, leading to oxidative stress and lipid peroxidation, which contribute to hepatotoxicity and nephrotoxicity [26]. CDDP treatment decreases the activity of antioxidant enzymes such as superoxide dismutase and catalase, while increasing lipid peroxidation [64]. As shown in Table 9, treatment with HA-MSN-CDDP significantly restored SOD and CAT activities and reduced TBARS levels compared to free CDDP, indicating effective protection against oxidative damage. These results demonstrate that HA-MSN-CDDP not only reduces systemic and renal toxicity but also alleviates oxidative stress through preservation of antioxidant enzyme activities. Furthermore, biochemical findings supported the histopathological analyses.

Table 8. Biochemical parameters of mice in experimental groups. Data are presented as mean ± SD.

Biochemical Parameters	Groups			
	Control (SF)	**CDDP**	**MSN-CDDP**	**HA-MSN-CDDP**
Total Protein (g/dL)	5.3 ± 0.29	5.5 ± 0.30	4.9 ± 0.15	5.0 ± 0.45
ALB (g/dL)	2.3 ± 0.12	2.4 ± 0.20	2.1 ± 0.16	2.5 ± 0.25
GLOB (g/dL)	3.0 ± 0.22	3.1 ± 0.15	2.8 ± 0.21	2.7 ± 0.19
GLU (mg/dL)	154 ± 10.1	114 ± 15.8	163 ± 11.6	171 ± 10.4
ALT (U/L)	42 ± 3.55	37 ± 5.18	44 ± 12.2	56 ± 3.61
ALP (U/L)	63.0 ± 4.81	77 ± 8.54	36 ± 5.15	<14
GGT (U/L)	<10	<10	<10	<10
TBIL (mg/dL)	1.3 ± 0.32	2.0 ± 0.23	1.4 ± 0.18	0.7 ± 0.25
TCHO (mg/dL)	64 ± 6.80	64 ± 4.75	65 ± 3.24	52 ± 7.52
CRE (mg/dL)	0.77 ± 0.21	0.85 ± 0.10	0.82 ± 0.09	0.52 ± 0.26
BUN (mg/dL)	41.9 ± 1.28	43.3 ± 1.54	31.8 ± 0.09	27.4 ± 0.11
Ca (mg/dL)	10.3 ± 1.05	9.4 ± 0.51	9.5 ± 1.12	7.7 ± 1.18
Inorganic P (mg/dL)	8.2 ± 0.13	7.9 ± 0.81	6.9 ± 0.35	7.5 ± 0.32

Table 9. SOD, CAT and lipid peroxidation levels of mice in experimental groups.

Treatment Groups	SOD (U/mg Protein)	CAT (U/mg Protein)	Lipid Peroxidation (nmol/mg Protein)
Lung			
Control (SF)	0.442 ± 0.028 $^{\#}$	0.822 ± 0.018 $^{\#}$	0.035 ± 0.008 $^{\#}$
CDDP	0.233 ± 0.027 *	1.111 ± 0.027 *	0.050 ± 0.009 *
MSN-CDDP	0.186 ± 0.016 *$^{\#}$	0.348 ± 0.030 *$^{\#}$	0.020 ± 0.002 *$^{\#}$
HA-MSN-CDDP	0.173 ± 0.015 *$^{\#}$	0.505 ± 0.028 *$^{\#}$	0.027 ± 0.003 $^{\#}$
F	12.065	487.130	12.104
P	0.000	0.000	0.002
Liver			
Control (SF)	0.120 ± 0.070 $^{\#}$	0.180 ± 0.011 $^{\#}$	0.020 ± 0.003 $^{\#}$
CDDP	0.076 ± 0.030 *	0.389 ± 0.049 *	0.032 ± 0.009 *
MSN-CDDP	0.094 ± 0.021 *	0.463 ± 0.020 *$^{\#}$	0.020 ± 0.001 $^{\#}$
HA-MSN-CDDP	0.198 ± 0.041 *$^{\#}$	0.520 ± 0.016 *$^{\#}$	0.017 ± 0.002 $^{\#}$
F	5.018	81.981	4.962
P	0.036	0.000	0.031
Kidney			
Control (SF)	0.106 ± 0.029 $^{\#}$	0.362 ± 0.021 $^{\#}$	0.052 ± 0.002 $^{\#}$
CDDP	0.077 ± 0.010 *	0.503 ± 0.020 *	0.100 ± 0.005 *
MSN-CDDP	0.176 ± 0.018 *$^{\#}$	0.538 ± 0.028 *	0.217 ± 0.018 *$^{\#}$
HA-MSN-CDDP	0.122 ± 0.016 $^{\#}$	0.480 ± 0.022 *$^{\#}$	0.128 ± 0.003 *$^{\#}$
F	22.006	41.742	141.399
P	0.000	0.000	0.000

* Statistically significant difference compared to the control group ($p < 0.05$). $^{\#}$ Statistically significant difference compared to the CDDP group ($p < 0.05$).

3.3.3. Histological and Immunohistochemical Evaluation

Histological analyses of lungs, liver, and kidney tissues were performed using routine hematoxylin–eosin (H&E) staining. Both stromal and parenchymal regions were examined for potential histological alterations (Figure 5). In lung tissue, the bronchiolar epithelia and most alveoli appeared normal in the control (SF) group. However, occasional interalveolar congestion, alveolar wall thickening, edema accumulation, and inflammation were observed in some alveoli. Extensive bronchiolar epithelial degeneration and luminal epithelial debris were observed in the CDDP treatment group. Only a few alveoli were of normal appearance, whereas widespread inflammation, edema, congestion, intraalveolar hemorrhage foci, and focal atelectasis were noted. Inflammation in perivascular and peribronchiolar areas was significantly reduced in the MSN-CDDP treatment group. Bronchiolar epithelial degeneration was limited to a small number of cells. Interalveolar inflammation and edema were minimal, and intra-alveolar hemorrhage and atelectasis were absent. On the other hand, bronchioles and alveoli appeared normal in the HA-MSN-CDDP treatment group, while only minor, localized inflammation foci were observed. In kidney tissue, glomeruli, tubules, interstitium, and blood vessels appeared normal in the control (SF) group. Severe alterations were noted, including hyaline deposits in proximal tubules leading to narrowed tubular lumens, dilated lumens with epithelial debris, degenerate glomeruli, loss of microvilli, and proximal tubular epithelial degeneration in the CDDP treatment group. Also, widespread interstitial inflammation was observed in this group. Mild atypical morphological changes occurred in some proximal and distal tubular epithelial cells, with slight lumen narrowing in the MSN-CDDP treatment group, while glomeruli and interstitial areas remained normal. No histological changes were detected in the HA-MSN-CDDP treatment group. When comparing the control group, glomeruli, tubules, interstitium, and blood vessels were of normal appearance in this group. In liver tissue, no histological changes were observed in any group, with normal portal triads, sinusoidal areas, and hepatocytes across all samples. In our study, HA-MSN-CDDP reduces CDDP-induced nephrotoxicity. This effect is attributed to the CD44-specific targeting of HA, which directs the nanoparticles toward A549-Luc-C8 tumor cells, and the controlled release of CDDP at the tumor site. In contrast, free chemotherapeutics often induce off-target side effects in healthy organs. By employing HA-modified, drug-loaded nanoparticles, it is possible to simultaneously achieve effective antitumor activity and minimize systemic toxicity, offering a safer and more efficient therapeutic strategy [15,16,54,60,61].

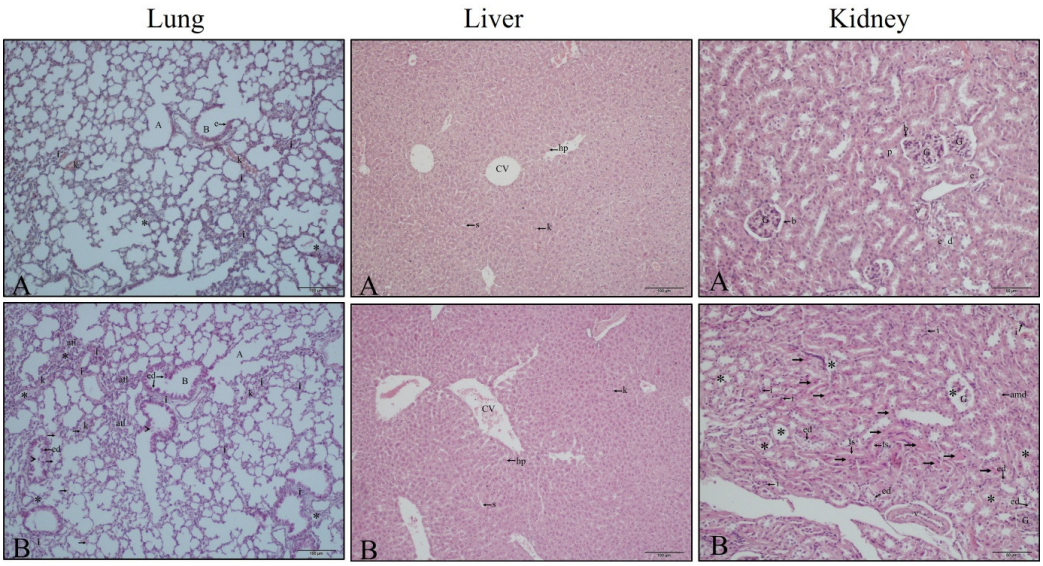

Figure 5. *Cont.*

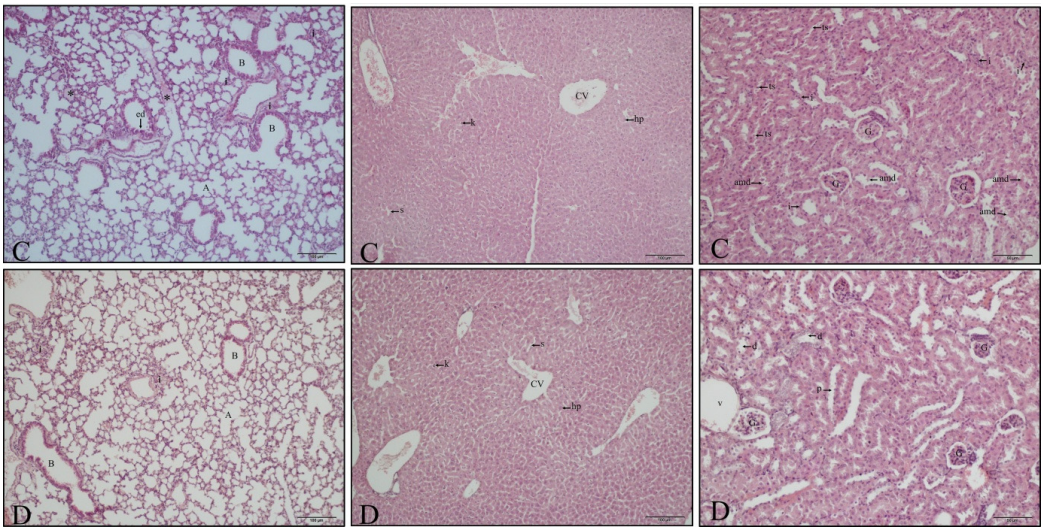

Figure 5. Histological images of lungs, liver and kidney tissues (H&E staining). Experimental groups: (**A**) SF; (**B**) CDDP; (**C**) MSN-CDDP; (**D**) HA-MSN-CDDP. Lung (B: bronchioles; A: alveoli; e: epithelium; ed: epithelial degeneration; arrow: interalveolar hemorrhage; arrowhead: epithelial eruptions; k: congestion; asterix (*): edema; i: inflammation; atl: atelectasis). Magnification: ×10, bar 100 µm; liver (CV: central vein; h: hepatocyte; k: Kupfer cell; s: sinusoid). Magnification: ×10, bar 100 µm; kidney (G: glomerulus; b: Bowman capsule; e: tubule epithelial cell; p: proximal tubule; d: distal tubule; v: vein; asterix: tubular and glomerular degeneration; arrow: increased proximal tubule hyaline cylinder: ed: cytoplasmic vacuolization and tubule epithelial degeneration; i: inflammation; amd: atypical morphological change; ts: tubular stenosis). Magnification: ×20, bar 50 µm.

Ki67 immunohistochemical analysis was performed to assess cell proliferation in lungs, liver, and kidney tissues across all experimental groups (Figure 6). In lung tissue, the SF group exhibited the highest number of Ki67-positive cells, indicating elevated proliferation, whereas the CDDP group showed a reduced expression, and the HA-MSN-CDDP group demonstrated the lowest Ki67 expression. Similarly, in liver and kidney tissues, Ki67 expression was highest in the SF group and lowest in the HA-MSN-CDDP group, suggesting that HA-MSN-CDDP effectively suppresses abnormal cell proliferation in both tumor and healthy tissues. Likewise, HA-modified NPs have effectively inhibited metastasis [52].

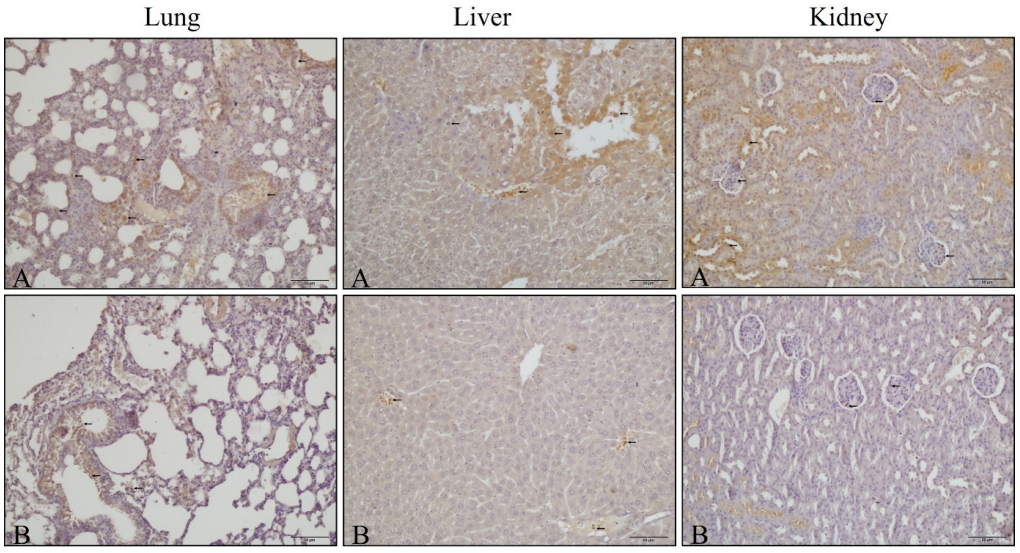

Figure 6. *Cont.*

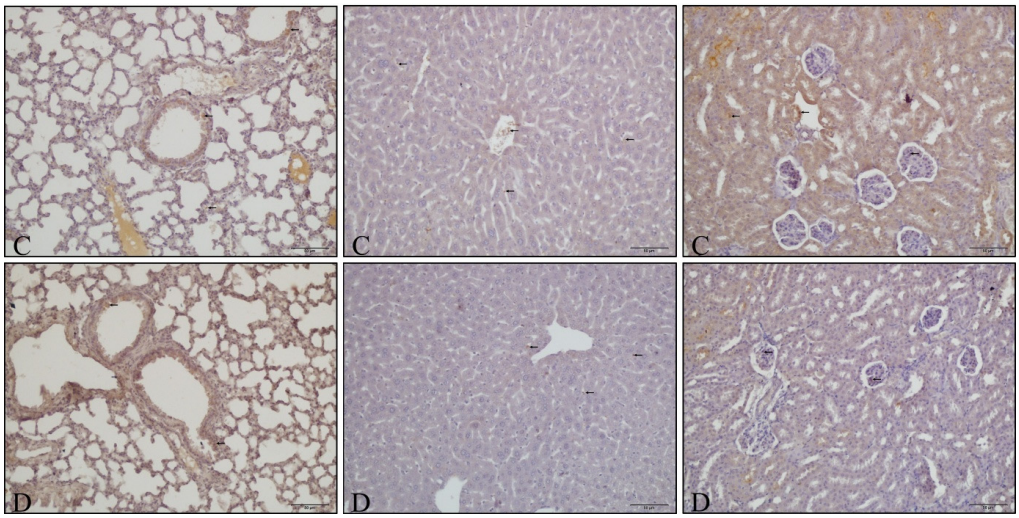

Figure 6. Ki67 immunohistochemistry expressions in lung, liver, and kidney tissues. Experimental groups: (**A**) SF; (**B**) CDDP; (**C**) MSN-CDDP; (**D**) HA-MSN-CDDP. Arrow: cells expressing Ki67. Magnification: ×20, bar 50 μm.

4. Conclusions

Over the past decade, numerous anticancer drug delivery systems have been developed using NPs functionalized with low-molecular-weight hyaluronic acid (LMWHA) to achieve tumor-specific targeting. In contrast, the present study is the first to demonstrate the successful synthesis and characterization of high-molecular-weight hyaluronic acid-functionalized, cisplatin-loaded mesoporous silica nanoparticles (HA-MSN-CDDP) designed for active CD44-mediated delivery of CDDP. The HA-MSN-CDDP formulation exhibited controlled cisplatin release and enhanced cellular uptake in CD44-overexpressing A549-Luc-C8 lung adenocarcinoma cells. In vitro assays confirmed that HA-MSN-CDDP significantly reduced the undesired cytotoxic, genotoxic, and oxidative stress-inducing effects of free CDDP on healthy cells while markedly increasing apoptosis in the cancer cells. Moreover, the HA-modified NP system showed excellent hemocompatibility, indicating its suitability for intravenous administration. In the xenograft lung cancer mouse model, HA-MSN-CDDP effectively inhibited tumor growth, prevented body weight loss, and maintained antioxidant enzyme activity compared to free CDDP. Histological analyses further demonstrated that HA-MSN-CDDP alleviated cisplatin-induced nephrotoxicity, confirming its biocompatibility and organ-protective effects. Collectively, these findings indicate that HA-MSN-CDDP represents a promising targeted chemotherapy platform for lung cancer treatment. Its high biocompatibility, controlled drug release, and efficient tumor suppression make it a valuable candidate for further preclinical and clinical development in precision nanomedicine.

Author Contributions: Conceptualization, C.G., D.O. and N.Ü.K.Y.; methodology, A.N., A.G., E.İ.M., A.Y., D.O. and N.Ü.K.Y.; software, N.Ü.K.Y.; validation, A.N., E.İ.M., A.Y., D.O. and N.Ü.K.Y.; formal analysis, C.G., S.S.G., E.Ş., A.B., H.E.T. and A.G.; investigation, C.G. and N.Ü.K.Y.; resources, N.Ü.K.Y., A.N., D.O. and A.Y.; data curation, C.G., A.Y. and N.Ü.K.Y.; writing—original draft preparation, C.G.; writing—review and editing, C.G., A.Y. and N.Ü.K.Y.; visualization, C.G., H.E.T., A.Y. and N.Ü.K.Y.; supervision, A.N., E.İ.M., A.Y., D.O. and N.Ü.K.Y.; project administration, N.Ü.K.Y.; funding acquisition, C.G. and N.Ü.K.Y. All authors have read and agreed to the published version of the manuscript.

Funding: This study is based on the PhD thesis of Dr. Cem Güler, who was supported by TUBITAK 2211C National PhD Scholarship Programs (Priority area: Biotechnological Drug Technologies) and 100/2000 CoHE PhD Scholarship Program (Priority area: Molecular Pharmacology and Drug

Research). This study was funded by Ege University Scientific Research Projects (FM-ÖNAP-2023-28473).

Institutional Review Board Statement: The experimental procedures were approved by the Ege University, Local Ethical Committee of Animal Experiment (approval date: 27 February 2022 and approval No. 2021-026). All procedures were conducted in accordance with the ARRIVE Guideline 2.0.

Informed Consent Statement: Not applicable.

Data Availability Statement: The raw data supporting the conclusions of this article will be made available by the authors on request.

Acknowledgments: The Authors thank Alper Akkaya from Ege University Department of Biochemistry and Nihal S. Tabasi from the Department of Chemistry for their contributions.

Conflicts of Interest: The authors declare no conflicts of interest. The funders had no role in the design of this study; in the collection, analyses, or interpretation of data; in the writing of the manuscript; or in the decision to publish the results.

References

1. Hendriks, L.E.; Remon, J.; Faivre-Finn, C.; Garassino, M.C.; Heymach, J.V.; Kerr, K.M.; Tan, D.S.; Veronesi, G.; Reck, M. Non-small-cell lung cancer. *Nat. Rev. Dis.* **2024**, *10*, 71. [CrossRef]
2. Sharma, P.; Mehta, M.; Dhanjal, D.S.; Kaur, S.; Gupta, G.; Singh, H.; Thangavelu, L.; Rajeshkumar, S.; Tambuwala, M.; Bakshi, H.A.; et al. Emerging trends in the novel drug delivery approaches for the treatment of lung cancer. *Chem.-Biol. Interact.* **2019**, *309*, 108720. [CrossRef] [PubMed]
3. Yetisgin, A.A.; Cetinel, S.; Zuvin, M.; Kosar, A.; Kutlu, O. Therapeutic nanoparticles and their targeted delivery applications. *Molecules* **2020**, *25*, 2193. [CrossRef]
4. Alyassin, Y.; Sayed, E.G.; Mehta, P.; Ruparelia, K.; Arshad, M.S.; Rasekh, M.; Shepherd, J.; Kucuk, I.; Wilson, P.B.; Singh, N.; et al. Application of mesoporous silica nanoparticles as drug delivery carriers for chemotherapeutic agents. *Drug Discov. Today* **2020**, *25*, 1513–1520. [CrossRef]
5. Li, Y.; Yan, B.; He, S. Advances and challenges in the treatment of lung cancer. *Biomed. Pharmacother.* **2023**, *169*, 115891. [CrossRef]
6. Ilyes, G.M.; Chahinez, B.; Saidi-Besbes, S.; Elaissari, A. Advances in mesoporous silica nanoparticles as carriers for drug delivery and other biomedical applications. *Microporous Mesoporous Mater* **2025**, *391*, 113603. [CrossRef]
7. Ahmed, H.; Gomte, S.S.; Prathyusha, E.; Agrawal, M.; Alexander, A. Biomedical applications of mesoporous silica nanoparticles as a drug delivery carrier. *J. Drug Deliv. Technol.* **2022**, *76*, 103729. [CrossRef]
8. Watermann, A.; Brieger, J. Mesoporous silica nanoparticles as drug delivery vehicles in cancer. *Nanomaterials* **2017**, *7*, 189. [CrossRef] [PubMed]
9. Manzano, M.; Vallet-Regí, M. Mesoporous silica nanoparticles for drug delivery. *Adv. Funct. Mater.* **2020**, *30*, 1902634. [CrossRef]
10. Salwowska, N.M.; Bebenek, K.A.; Żądło, D.A.; Wcisło-Dziadecka, D.L. Physiochemical properties and application of hyaluronic acid: A systematic review. *Cosmet. Dermatol.* **2016**, *15*, 520–526. [CrossRef]
11. D'Agostino, A.; Stellavato, A.; Corsuto, L.; Diana, P.; Filosa, R.; La Gatta, A.; De Rosa, M.; Schiraldi, C. Is molecular size a discriminating factor in hyaluronan interaction with human cells? *Carbohydr. Polym.* **2017**, *157*, 21–30. [CrossRef] [PubMed]
12. Kim, K.; Choi, H.; Choi, E.S.; Park, M.H.; Ryu, J.H. Hyaluronic acid-coated nanomedicine for targeted cancer therapy. *Pharmaceutics* **2019**, *11*, 301. [CrossRef]
13. Kesharwani, P.; Chadar, R.; Sheikh, A.; Rizg, W.Y.; Safhi, A.Y. CD44-targeted nanocarrier for cancer therapy. *Front. Pharmacol.* **2022**, *12*, 800481. [CrossRef]
14. Yu, M.; Jambhrunkar, S.; Thorn, P.; Chen, J.; Gu, W.; Yu, C. Hyaluronic acid modified mesoporous silica nanoparticles for targeted drug delivery to CD44-overexpressing cancer cells. *Nanoscale* **2013**, *5*, 178–183. [CrossRef]
15. Zhong, Y.; Zhang, J.; Cheng, R.; Deng, C.; Meng, F.; Xie, F.; Zhong, Z. Reversibly crosslinked hyaluronic acid nanoparticles for active targeting and intelligent delivery of doxorubicin to drug resistant CD44+ human breast tumor xenografts. *J. Control. Release* **2015**, *205*, 144–154. [CrossRef] [PubMed]
16. Wu, J.; Deng, C.; Meng, F.; Zhang, J.; Sun, H.; Zhong, Z. Hyaluronic acid coated PLGA nanoparticulate docetaxel effectively targets and suppresses orthotopic human lung cancer. *J. Control. Release* **2017**, *259*, 76–82. [CrossRef]
17. Gupta, B.; Poudel, B.K.; Ruttala, H.B.; Regmi, S.; Pathak, S.; Gautam, M.; Jin, S.G.; Jeong, J.-H.; Choi, H.-G.; Ku, S.K.; et al. Hyaluronic acid-capped compact silica-supported mesoporous titania nanoparticles for ligand-directed delivery of doxorubicin. *Acta Biomater.* **2018**, *80*, 364–377. [CrossRef]

18. Zarkesh, K.; Heidari, R.; Iranpour, P.; Azarpira, N.; Ahmadi, F.; Mohammadi-Samani, S.; Farjadian, F. Theranostic hyaluronan coated EDTA modified magnetic mesoporous silica nanoparticles for targeted delivery of cisplatin. *J. Drug Deliv. Technol.* **2022**, *77*, 103903. [CrossRef]
19. Munderere, R.; Gulfam, M.; Ali, I.; Kim, S.H.; Vu, T.T.; Park, S.H.; Lim, K.T. Redox-responsive gold nanoparticles coated with hyaluronic acid and folic acid for application in targeting anticancer therapy. *Molecules* **2024**, *29*, 1564. [CrossRef]
20. Pakian, S.; Mirkani, A.; Sadeghi-Abandansari, H.; Nabid, M.R. Stabilization of cationic liposomes using hyaluronic acid-modified gold nanoparticles by post-microfluidics conjugation approach for drug delivery applications. *J. Drug Deliv. Technol.* **2024**, *99*, 105956. [CrossRef]
21. Soleymani, M.; Velashjerdi, M.; Asgari, M. Preparation of hyaluronic acid-decorated mixed nanomicelles for targeted delivery of hydrophobic drugs to CD44-overexpressing cancer cells. *Int. J. Pharm.* **2021**, *592*, 120052. [CrossRef]
22. Espinosa-Cano, E.; Huerta-Madronal, M.; Camara-Sanchez, P.; Seras-Franzoso, J.; Schwartz, S., Jr.; Abasolo, I.; Roman, J.S.; Aguilar, M.R. Hyaluronic acid (HA)-coated naproxen-nanoparticles selectively target breast cancer stem cells through COX-independent pathways. *Mater. Sci. Eng. C* **2021**, *124*, 112024. [CrossRef]
23. Almoustafa, H.A.; Alshawsh, M.A.; Al-Suede, F.S.R.; Alshehade, S.A.; Abdul Majid, A.M.S.; Chik, Z. The chemotherapeutic efficacy of hyaluronic acid coated polymeric nanoparticles against breast cancer metastasis in female NCr-Nu/Nu nude mice. *Polymers* **2023**, *15*, 284. [CrossRef]
24. Chen, H.A.; Lu, Y.J.; Dash, B.S.; Chao, Y.K.; Chen, J.P. Hyaluronic acid-modified cisplatin-encapsulated poly (lactic-co-glycolic acid) magnetic nanoparticles for dual-targeted NIR-responsive chemo-photothermal combination cancer therapy. *Pharmaceutics* **2023**, *15*, 290. [CrossRef]
25. Aasy, N.K.A.; Sallam, M.A.; Ragab, D.; Abdelmonsif, D.A.; Aly, R.G.; Abdelfattah, E.Z.A.; Elkhodairy, K.A. CD44-targeted hyaluronic acid coated imiquimod lipid nanocapsules foster the efficacy against skin cancer: Attempt to conquer unfavorable side effects. *Int. J. Biol. Macromol.* **2025**, *290*, 138895. [CrossRef] [PubMed]
26. Ghosh, S. Cisplatin: The first metal based anticancer drug. *Bioorg. Chem.* **2019**, *88*, 102925. [CrossRef] [PubMed]
27. Elmorsy, E.A.; Saber, S.; Hamad, R.S.; Abdel-Reheim, M.A.; El-Kott, A.F.; AlShehri, M.A.; Morsy, K.; Salama, S.A.; Youssef, M.E. Advances in understanding cisplatin-induced toxicity: Molecular mechanisms and protective strategies. *Eur. J. Pharm. Sci.* **2024**, *203*, 106939. [CrossRef] [PubMed]
28. Ichedef, Ç.; Aydın, B.; Hamurişçi, S.İ.; Teksöz, S.; Medine, E.İ. A promising radiolabeled drug delivery system for methotrexate: Synthesis and in vitro evaluation of 99mTc labeled drug loaded uniform mesoporous silica nanoparticles. *J. Radioanal. Nucl.* **2021**, *330*, 1113–1125. [CrossRef]
29. Huang, L.; Liu, M.; Mao, L.; Huang, Q.; Huang, H.; Zeng, G.; Tian, J.; Wen, Y.; Zhang, X.; Wei, Y. A facile FeBr3 based photoATRP for surface modification of mesoporous silica nanoparticles for controlled delivery cisplatin. *Appl. Surf. Sci.* **2018**, *434*, 204–210. [CrossRef]
30. Joyce, P.; Ulmefors, H.; Maghrebi, S.; Subramaniam, S.; Wignall, A.; Jõemetsa, S.; Höök, F.; Prestidge, C.A. Enhancing the cellular uptake and antibacterial activity of rifampicin through encapsulation in mesoporous silica nanoparticles. *Nanomaterials* **2020**, *10*, 815. [CrossRef]
31. Mosmann, T. Rapid colorimetric assay for cellular growth and survival: Application to proliferation and cytotoxicity assays. *J. Immunol. Methods* **1983**, *65*, 55–63. [CrossRef] [PubMed]
32. Guler, C.; Gulcemal, S.; Guner, A.; Akgol, S.; Karabay Yavasoglu, N.U. Polymeric nanoparticles tryptophan-graft-p (HEMA): A study on synthesis, characterization, and toxicity. *Polym. Bull.* **2023**, *80*, 10973–10996. [CrossRef]
33. Maron, D.M.; Ames, B.N. Revised methods for the Salmonella mutagenicity test. *Mutat. Res. Environ. Mutagen. Relat. Subj.* **1983**, *113*, 173–215. [CrossRef]
34. Percie du Sert, N.; Hurst, V.; Ahluwalia, A.; Alam, S.; Avey, M.T.; Baker, M.; Browne, W.J.; Clark, A.; Cuthill, I.C.; Dirnagl, U.; et al. The ARRIVE guidelines 2.0: Updated guidelines for reporting animal research. *Br. J. Pharmacol.* **2020**, *177*, 3617–3624. [CrossRef]
35. Cheng, Y.L.; Lee, S.C.; Lin, S.Z.; Chang, W.L.; Chen, Y.L.; Tsai, N.M.; Liu, Y.-C.; Tzao, C.; Yu, D.-S.; Harn, H.J. Anti-proliferative activity of Bupleurum scrozonerifolium in A549 human lung cancer cells in vitro and in vivo. *Cancer Lett.* **2005**, *222*, 183–193. [CrossRef]
36. Li, X.; Li, R.; Qian, X.; Ding, Y.; Tu, Y.; Guo, R.; Hu, Y.; Jiang, X.; Guo, W.; Liu, B. Superior antitumor efficiency of cisplatin-loaded nanoparticles by intratumoral delivery with decreased tumor metabolism rate. *Eur. J. Pharm.* **2008**, *70*, 726–734. [CrossRef]
37. Bradford, M.M. A rapid and sensitive method for the quantiza- tion of microgram quantities of protein utilizing the principle of protein-dye binding. *Anal Biochem.* **1976**, *72*, 248–254. [CrossRef] [PubMed]
38. Ewing, J.F.; Janero, D.R. Microplate superoxide dismutase assay employing a nonenzymatic superoxide generator. *Anal. Biochem.* **1995**, *232*, 243–248. [CrossRef] [PubMed]
39. Beers, R.F., Jr.; Sizer, I.W. A spectrophotometric method for measur- ing the breakdown of hydrogen peroxide by catalase. *J. Biol. Chem.* **1951**, *195*, 133–140. [CrossRef]

40. Ohkawa, H.; Ohishi, N.; Yagi, K. Assay for lipid peroxides in animal tissues by thiobarbituric acid reaction. *Anal. Biochem.* **1979**, *95*, 351–358. [CrossRef]
41. Ma, M.; Chen, H.; Chen, Y.; Zhang, K.; Wang, X.; Cui, X.; Shi, J. Hyaluronic acid-conjugated mesoporous silica nanoparticles: Excellent colloidal dispersity in physiological fluids and targeting efficacy. *J. Mater. Chem.* **2012**, *22*, 5615–5621. [CrossRef]
42. Fan, X.; Wang, T.; Han, M.; Gu, Y.; Sun, G.; Peng, X.; Shou, Q.; Song, H.; Liu, W.; Nian, R. Dual CEA/CD44 targeting to colorectal cancer cells using nanobody-conjugated hyaluronic acid-modified mesoporous silica nanoparticles with pH-and redox-sensitivity. *Mater. Adv.* **2022**, *3*, 4707–4717. [CrossRef]
43. Chen, Z.; Li, Z.; Lin, Y.; Yin, M.; Ren, J.; Qu, X. Bioresponsive hyaluronic acid-capped mesoporous silica nanoparticles for targeted drug delivery. *Chem.—Eur. J.* **2013**, *19*, 1778–1783. [CrossRef]
44. Nairi, V.; Magnolia, S.; Piludu, M.; Nieddu, M.; Caria, C.A.; Sogos, V.; Vallet-Regì, M.; Monduzzi, M.; Salis, A. Mesoporous silica nanoparticles functionalized with hyaluronic acid. Effect of the biopolymer chain length on cell internalization. *Colloids Surf. B Biointerfaces* **2018**, *168*, 50–59. [CrossRef]
45. Rizvi, S.A.; Saleh, A.M. Applications of nanoparticle systems in drug delivery technology. *SPJ* **2018**, *26*, 64–70. [CrossRef]
46. Adabi, M.; Naghibzadeh, M.; Adabi, M.; Zarrinfard, M.A.; Esnaashari, S.S.; Seifalian, A.M.; Faridi-Majidi, R.; Aiyelabegan, H.T.; Ghanbari, H. Biocompatibility and nanostructured materials: Applications in nanomedicine. *Artif. Cells Nanomed. Biotechnol.* **2017**, *45*, 833–842. [CrossRef] [PubMed]
47. Egbuna, C.; Parmar, V.K.; Jeevanandam, J.; Ezzat, S.M.; Patrick-Iwuanyanwu, K.C.; Adetunji, C.O.; Khan, J.; Onyeike, E.N.; Uche, C.Z.; Akram, M.; et al. Toxicity of nanoparticles in biomedical application: Nanotoxicology. *J. Toxicol.* **2021**, *2021*, 9954443. [CrossRef] [PubMed]
48. Kestens, V.; Roebben, G.; Herrmann, J.; Jämting, Å.; Coleman, V.; Minelli, C.; Clifford, C.; De Temmerman, P.-J.; Mast, J.; Junjie, L.; et al. Challenges in the size analysis of a silica nanoparticle mixture as candidate certified reference material. *J. Nanoparticle Res.* **2016**, *18*, 171. [CrossRef]
49. Yusuf, A.; Almotairy, A.R.Z.; Henidi, H.; Alshehri, O.Y.; Aldughaim, M.S. Nanoparticles as drug delivery systems: A review of the implication of nanoparticles' physicochemical properties on responses in biological systems. *Polymers* **2023**, *15*, 1596. [CrossRef]
50. Kousar, K.; Naseer, F.; Abduh, M.S.; Kakar, S.; Gul, R.; Anjum, S.; Ahmad, T. Green synthesis of hyaluronic acid coated, thiolated chitosan nanoparticles for CD44 targeted delivery and sustained release of Cisplatin in cervical carcinoma. *Front. Pharmacol.* **2023**, *13*, 1073004. [CrossRef]
51. Wang, X.; Song, Y.; Yu, L.; Xue, X.; Pang, M.; Li, Y.; Luo, X.; Hua, Z.; Lu, C.; Lu, A.; et al. Co-delivery of hesperetin and cisplatin via hyaluronic acid-modified liposome for targeted inhibition of aggression and metastasis of triple-negative breast cancer. *ACS Appl. Mater. Interfaces* **2023**, *15*, 34360–34377. [CrossRef]
52. Gong, T.; Dong, Z.; Fu, Y.; Gong, T.; Deng, L.; Zhang, Z. Hyaluronic acid modified doxorubicin loaded Fe_3O_4 nanoparticles effectively inhibit breast cancer metastasis. *J. Mater. Chem. B* **2019**, *7*, 5861–5872. [CrossRef]
53. Gotov, O.; Battogtokh, G.; Shin, D.; Ko, Y.T. Hyaluronic acid-coated cisplatin conjugated gold nanoparticles for combined cancer treatment. *JIEC* **2018**, *65*, 236–243. [CrossRef]
54. Hu, Y.; Zhang, J.; Dong, L.; Xu, L.; Chen, E. DOX-loaded mesoporous hydroxyapatite modified by hyaluronic acid can achieve efficient targeted therapy for lung cancer. *J. Drug Target.* **2023**, *31*, 612–622. [CrossRef] [PubMed]
55. Hannan, M.A.; Al-Dakan, A.A.; Hussain, S.S.; Amer, M.H. Mutagenicity of cisplatin and carboplatin used alone and in combination with four other anticancer drugs. *Toxicology* **1989**, *55*, 183–191. [CrossRef] [PubMed]
56. Ferreira, N.H.; Furtado, R.A.; Ribeiro, A.B.; de Oliveira, P.F.; Ozelin, S.D.; de Souza, L.D.R.; Neto, F.R.; Miura, B.A.; Magalhães, G.M.; Nassar, E.J.; et al. Europium (III)-doped yttrium vanadate nanoparticles reduce the toxicity of cisplatin. *J. Inorg. Biochem.* **2018**, *182*, 9–17. [CrossRef]
57. Slowing, I.I.; Wu, C.W.; Vivero-Escoto, J.L.; Lin, V.S.Y. Mesoporous silica nanoparticles for reducing hemolytic activity towards mammalian red blood cells. *Small* **2009**, *5*, 57–62. [CrossRef]
58. Lin, Y.S.; Haynes, C.L. Impacts of mesoporous silica nanoparticle size, pore ordering, and pore integrity on hemolytic activity. *J. Am. Chem. Soc.* **2010**, *132*, 4834–4842. [CrossRef]
59. Zhong, Y.; Goltsche, K.; Cheng, L.; Xie, F.; Meng, F.; Deng, C.; Zhong, Z.; Haag, R. Hyaluronic acid-shelled acid-activatable paclitaxel prodrug micelles effectively target and treat CD44-overexpressing human breast tumor xenografts in vivo. *Biomaterials* **2016**, *84*, 250–261. [CrossRef]
60. Wang, X.; Cheng, R.; Zhong, Z. Facile fabrication of robust, hyaluronic acid-surfaced and disulfide-crosslinked PLGA nanoparticles for tumor-targeted and reduction-triggered release of docetaxel. *Acta Biomater.* **2021**, *125*, 280–289. [CrossRef] [PubMed]
61. Liu, S.; Tong, S.; Liu, G.; Wang, S.; Zhang, K.; Qiu, Z. Hyaluronic acid-functionalized nanoparticles enable enhanced chemo/chemodynamic therapy for the targeted treatment of colon cancer. *Int. J. Biol. Macromol.* **2025**, *303*, 140553. [CrossRef] [PubMed]

62. Charles River, BALB/c Nude Mouse Hematology, North American Colonies, January 2011–December 2012. Available online: https://www.google.com/url?sa=t&source=web&rct=j&opi=89978449&url=https://www.criver.com/resources/balbc-nude-mouse-clinical-pathology-data (accessed on 25 November 2025).
63. Perše, M. Cisplatin mouse models: Treatment, toxicity and translatability. *Biomedicines* **2021**, *9*, 1406. [CrossRef] [PubMed]
64. Husain, K.; Morris, C.; Whitworth, C.; Trammell, G.L.; Rybak, L.P.; Somani, S.M. Protection by ebselen against cisplatin-induced nephrotoxicity: Antioxidant system. *Mol. Cell. Biochem.* **1998**, *178*, 127–133. [CrossRef] [PubMed]